Comparative studies on two phases of Archaean TTG magmas from different blocks of the North China Craton: petrogenesis and constraints on crustal evolution

Original Article

Author for correspondence:
Houxiang Shan; Mingguo Zhai,
Emails: shanhouxiang@mail.iggcas.ac.cn;
mgzhai@mail.iggcas.ac.cn

Houxiang Shan[1,2,3] ![ORCID], Mingguo Zhai[3,4], RN Mitchell[3], Fu Liu[3] and Jinghui Guo[3]

[1]Key Laboratory of Active Tectonics and Volcano, Institute of Geology, China Earthquake Administration, Beijing 100029, China; [2]Key Laboratory of Mineral Resources, Institute of Geology and Geophysics, Chinese Academy of Sciences, Beijing 100029, China; [3]Innovation Academy for Earth Science, Chinese Academy of Sciences, Beijing 100029, China and [4]Key Laboratory of Computational Geodynamics, University of Chinese Academy of Sciences, Beijing 100049, China

Abstract

Whole-rock major and trace elements and Hf isotopes of magmatic zircons of tonalite–trondhjemite–granodiorite (TTG) rocks with different ages (2.9, 2.7 and 2.5 Ga) from the three blocks (the Eastern Block, Western Block and Trans-North China Orogen) of the North China Craton were compiled to investigate their respective petrogenesis, tectonic setting and implications for crustal growth and evolution. Geochemical features of the 2.5 Ga TTGs of the Eastern Block require melting of predominant rutile-bearing eclogite and subordinate garnet-amphibolite at higher pressure, while the source material of the 2.7 Ga TTGs is garnet-amphibolite or granulite at lower pressure. The 2.5 Ga TTGs have high Mg#, Cr and Ni, negative Nb–Ta anomalies and a juvenile basaltic crustal source, indicating derivation from the melting of a subducting slab. In contrast, features of the 2.7 Ga TTGs suggest generation from melting of thickened lower crust. The 2.5 and 2.7 Ga TTGs in the Trans-North China Orogen were formed at garnet-amphibolite to eclogite facies, and the source material of the 2.5 Ga TTGs in the Western Block is most likely garnet-amphibolite or eclogite. The 2.5 Ga TTGs in the Trans-North China Orogen and Western Block were generated by the melting of a subducting slab, whereas the 2.7 Ga TTGs in the Trans-North China Orogen derived from melting of thickened lower crust. The Hf isotopic data suggest both the 2.5 and 2.7 Ga TTG magmas were involved with contemporary crustal growth and reworking. The two-stage model age (T_{DM2}) histograms show major crustal growth between 2.9 and 2.7 Ga for the whole North China Craton.

1. Introduction

Tonalite–trondhjemite–granodiorite (TTG) suites, constituting up to ~80 % of Archaean terranes worldwide, are critical components of the ancient continental crust (Martin *et al.* 2005). Moreover, TTG magmatism represents an important transition in a terrane that links the original mafic crust with the subsequent crust of a potassic granitic composition (Glikson, 1979), because it is commonly considered that TTG rocks are generated by partial melting of hydrated basalts and are the parent rocks of many potassic granites. Therefore, TTGs represent an essential element in the 'protocontinental' stage of crustal growth and evolution (Barker, 1979), and thus can provide vital insights into understanding the crustal evolution and geodynamic regime.

A series of constraints from experimental petrology, phase equilibrium and geochemical studies have revealed that Archaean TTGs were generated by melting of hydrous metabasalts, but it is difficult to distinguish between melting of amphibolitic, garnet-amphibolitic or eclogitic sources (Arth & Hanson, 1972; Beard & Lofgren, 1991; Rapp *et al.* 1991, 2003; Foley *et al.* 2002, 2003; Xiong, 2006; Moyen & Stevens, 2006; Moyen, 2011). In addition, the geodynamic setting for TTGs is still debated, and no consensus has been reached between various models, which include: hot subduction (Drummond & Defant, 1990; Peacock *et al.* 1994; Martin, 1999; Martin *et al.* 2005), thickened lower crust (Atherton & Petford, 1993; Smithies, 2000; Whalen *et al.* 2002; Condie, 2005; Nair & Chacko, 2008; Nagel *et al.* 2012), delamination at the base of an oceanic plateau (Zegers & van Keken, 2001; Bedard, 2006) or the possible involvement of a mantle plume (Arndt & Goldstein, 1989; Kröner, 1991; Kröner & Layer, 1992; Condie, 2005; Willbold *et al.* 2009), and, furthermore, a new model involving the subduction of oceanic plateaus (Martin *et al.* 2014).

The North China Craton (NCC), the largest and oldest cratonic block in China (~3.8 Ga; Wu *et al.* 2008; Zhai & Santosh, 2011; Zhai, 2014 and references therein), carries a widespread
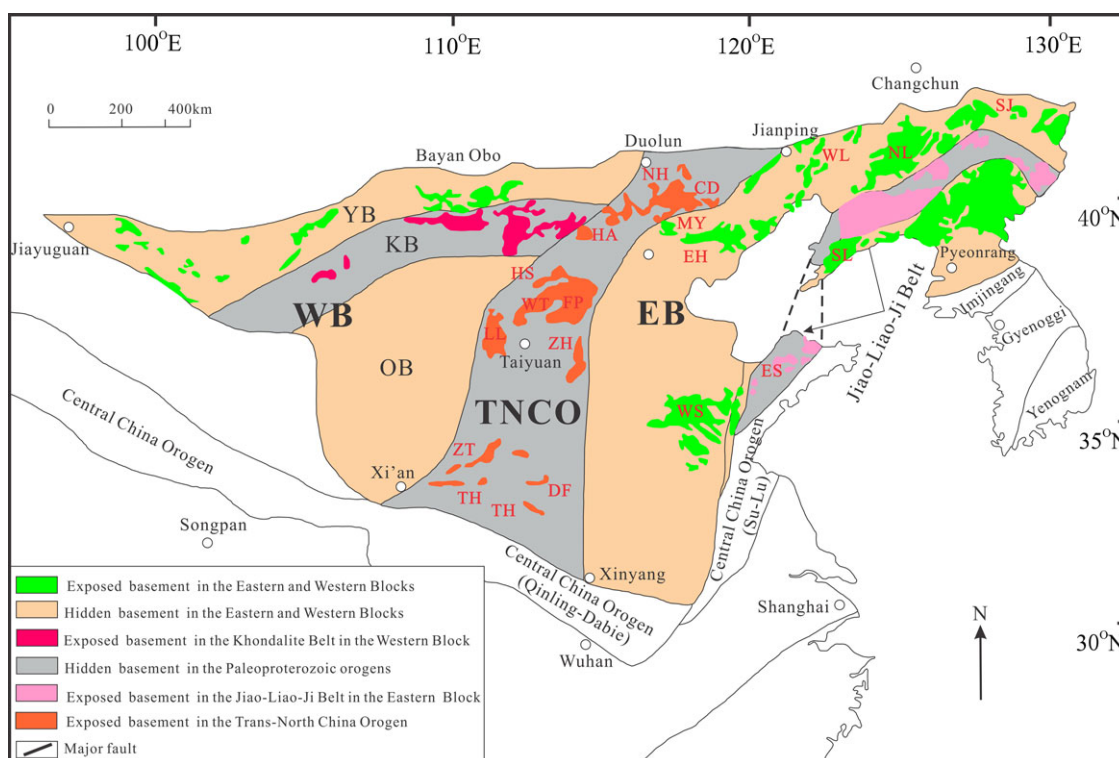
Fig. 1. (Colour online) Geological sketch map of the North China Craton (modified after Zhao et al. 2005). Abbreviations: YB – Yinshan Block; KB – Khondalite Belt; OB – Ordos Block; WB – Western Block; TNCO – Trans-North China Orogen; EB – Eastern Block; SJ – Southern Jilin; WL – Western Liaoning; NL – Northern Liaoning; SL – Southern Liaoning; CD – Chengde; DF – Dengfeng; MY – Miyun; NH – Northern Hebei; EH – Eastern Hebei; WT – Wutai; HS – Hengshan; FP – Fuping; HA – Huai'an; ZH – Zanhuang; LL – Lvliang; ES – Eastern Shandong; TH – Taihua; WS – Western Shandong; ZT – Zhongtiao.

Precambrian crystalline basement that predominantly comprises TTG gneisses. Therefore, the NCC is one of the best natural laboratories to study ancient crustal growth and evolution. In terms of substantive structural, geological, geochemical, geochronological and P–T data, the basement of the NCC can be tectonically divided into the Eastern Block (EB), the Western Block (WB) and the Trans-North China Orogen (TNCO) (Zhao et al. 2005). Previous studies have focused on the TTGs in specific areas of the NCC (see online Supplementary Material Tables S1–S4) and have proposed respective models to account for the petrogenesis and tectonic settings. However, a synthesis of the TTGs with different ages in each block is lacking, which hinders understanding the overall formation mechanism of the TTGs with different ages in each block and the geodynamic regime of crustal growth and reworking in the NCC. Therefore, in this study, we compile and synthesize the published geochemical data available, including whole-rock major and trace elements and zircon Lu–Hf isotopes of the TTGs with different ages from the basement rocks of the three blocks, in order to discuss the respective source and tectonic setting of these TTGs and then evaluate the crustal growth and evolution of the NCC. The results can possibly provide important constraints on the tectonic subdivision of the NCC.

2. Geologic setting

The NCC, the Chinese part of the Sino-Korean Craton, is the oldest and largest craton in China, with ancient crustal nuclei as old as 3.8 Ga (Liu et al. 1992; Wu et al. 2008; Zhai & Santosh, 2011; Zhai, 2014 and references therein). It covers an

area of c. 1 500 000 km^2 and is bounded by the early Palaeozoic Qilianshan Orogen to the west, the late Palaeozoic Tianshan-Xing'an Mongolian Orogen to the north and the Qinling–Dabie–Sulu ultrahigh pressure (UHP) metamorphic belt to the south. Although remarkable advances have been achieved by recent studies and a broad consensus has been reached in understanding the crustal evolution of the NCC, the tectonic subdivision and timing of amalgamation of the NCC remain disputed issues (Wu et al. 1998; Zhao et al. 1998, 1999a,b, 2000, 2001, 2005; Zhai et al. 2000; Kusky & Li, 2003; Kusky et al. 2007; Trap et al. 2008, 2009; Santosh, 2010; Santosh et al. 2010; Kusky, 2011; Zhai & Santosh, 2011; Zhao & Cawood, 2012; Zhao & Guo, 2012; Zheng et al. 2013). One of the most common subdivision methods is to divide the NCC into three major units: the EB (Eastern Block), WB (Western Block) and TNCO (Trans-North China Orogen) (Fig. 1; Zhao et al. 2005). The WB and EB were both formed by amalgamation of two crustal blocks, of which the WB is subdivided into the Yinshan Block in the north and the Ordos Block in the south by the E–W-trending Khondalite Belt (Fig. 1; Xia et al. 2006a,b, 2008; Zhao, 2009; Zhao et al. 2010; Wang et al. 2011). Similarly, the EB is taken as a collage of the Longgang Block to the north and the Nangrim Block to the south along the Jiao–Liao–Ji belt (Li et al. 2004, 2005, 2006, 2011b; Zhao et al. 2005; Li & Zhao, 2007; Luo et al. 2008).

2.a. Eastern Block

The Eastern Block is composed of the Eastern Hebei, Miyun–Chengde, Eastern Shandong, Western Shandong, Western Liaoning, Southern

Liaoning, Northern Liaoning and Southern Jilin domains (Fig. 1). The basement rocks of the EB consist primarily of pre-tectonic felsic gneisses (mainly TTG gneisses), syntectonic granitoids and minor supracrustal rocks that include ultramafic to mafic volcanic rocks and sedimentary rocks (including banded iron formations). Among the basement rocks are a large per cent of Neoarchaean lithological assemblages, with minor Eoarchaean to Paleoarchaean (3.8 Ga to 3.3 Ga) rocks (Jahn *et al.* 1987, 1988; Liu *et al.* 1992; Song *et al.* 1996; Nutman *et al.* 2009, 2011; Wan *et al.* 2009*a*). All of them were metamorphosed at greenschist- to granulite-facies conditions at 2.50–2.48 Ga with anticlockwise isobaric cooling (IBC)-type *P–T* paths (Wu *et al.* 2012). Geochronological data show that the dominant age ranges of the TTG gneisses and volcanic rocks are from 3.5 to 2.5 Ga (Zhao *et al.* 1998, 2001 and references therein), whereas the syntectonic granitoids were emplaced only at 2.5 Ga. In addition, 3.8 Ga crust has been identified in the Eastern Hebei and Anshan areas (e.g. Liu *et al.* 1992; Song *et al.* 1996), considered to be the oldest crustal remnants and the most primitive continental crust of the NCC.

2.b. Western Block

The Western Block is subdivided into the Yinshan Block in the north and the Ordos Block in the south by the Palaeoproterozoic Khondalite Belt that trends E–W and extends from western Helanshan and Qianlishan, through Daqingshan and Wulanshan, to the eastern Jining area (Zhao *et al.* 2005, 2011; Zhao, 2009; Santosh, 2010; Li *et al.* 2011*a*; Santosh *et al.* 2012). Investigations from Wu *et al.* (1986) showed that the Ordos Block is completely covered by the younger Ordos Basin. Therefore, the basement rocks of the WB are primarily exposed in the Yinshan Block and Khondalite Belt, including the Guyang–Wuchuan, Helanshan–Qianlishan, Daqingshan–Ulashan, Sheerteng and Jining areas (Fig. 1).

Represented by the Guyang and Wuchuan areas, the Yinshan Block is predominantly composed of late Archaean granitic (mainly TTG) gneisses and minor supracrustal rocks, all of which were metamorphosed at greenschist to granulite facies at ~2.5 Ga (Zhao *et al.* 1999*b* and references therein). The Khondalite Belt was the belt along which the Ordos and Yinshan blocks amalgamated to form the uniform WB at 1.95–1.92 Ga (Zhao *et al.* 2005, 2011; Santosh *et al.* 2006, 2007, 2009; Wan *et al.* 2006, 2009*a,b*; Yin *et al.* 2009, 2011; Zhao, 2009; Li *et al.* 2011*a*), the metamorphic evolution of which is characterized by clockwise isothermal decompression (ITD) *P–T* paths (Zhao *et al.* 1999*b*, 2005, 2011). However, the protolith age of the basement rocks in the Khondalite Belt remains controversial (Zhang *et al.* 1994; Lu *et al.* 1996). Some workers consider it could be Archaean (Qian & Li, 1999), whereas others take it to be Palaeoproterozoic (Zhao *et al.* 1999*b*; Wan *et al.* 2009*b*).

2.c. Trans-North China Orogen

The Trans-North China Orogen, including the Dengfeng, Fuping, Hengshan, Huai'an, Lvliang, Northern Hebei, Wutai, Zanhuang and Zhongtiao domains (Fig. 1), is separated from the EB and WB by major faults. It has been considered to be the collisional zone between the Eastern and Western blocks at ~1.8 Ga (Zhao *et al.* 2001). It is composed predominantly of Neoarchaean to Palaeoproterozoic basement rocks metamorphosed at greenschist to granulite facies. According to the lithology and metamorphic grade, the basement rocks of the TNCO have been divided into high-grade gneisses containing the Fuping, Hengshan and Huai'an areas and low-grade granite–greenstone belts including the Dengfeng, Lvliang, Wutai, Zhongtiao and Zanhuang domains (Zhao *et al.* 2000). The available geochronological data suggest that the

emplacement of the TTG and granitic plutons and eruption of mafic to felsic volcanic rocks mainly took place at 2.5–1.9 Ga with a major peak at ~2.5 Ga and a minor peak at ~2.1 Ga (e.g. Zhao *et al.* 2000, 2001, 2008; Guo *et al.* 2005; Kröner *et al.* 2005, 2006). Interestingly, all the basement rocks in the TNCO, regardless of their composition, protolith age and metamorphic grade, are characterized by clockwise ITD-type *P–T* paths, possibly related to the collision between the EB and WB (Zhao *et al.* 2000, 2010; Xiao *et al.* 2010). Extensive zircon SHRIMP U–Pb, monazite U–Pb, and mineral Ar–Ar and Sm–Nd dating indicate that the metamorphism in the TNCO happened at ~1.85 Ga (Guo & Zhai, 2001; Guo *et al.* 2005; Liu *et al.* 2006; Wan *et al.* 2006; Zhao *et al.* 2010, 2011 and references therein).

3. Data sources, filtering and illustration

Previous studies demonstrated that the magmatic ages of the TTGs in the EB and TNCO are predominantly ~2.5 Ga and ~2.7 Ga, whereas those in the WB are mostly concentrated around 2.5 Ga (online Supplementary Material Fig. S1; Zhai & Santosh, 2011). Therefore, the comparative studies conducted here are between the two phases of TTGs in the three blocks.

To accurately depict the TTGs in the three blocks of the NCC, we compiled geochemical analyses from a wide range of literature. A large database of Archaean gneissic and plutonic TTGs, including grey gneisses, TTG orthogneisses and TTG plutons was compiled for analysis. To make sure all the data used for the calculations and discussions agreed with the definition of TTGs, we filtered the database based on the TTG definition from Barker (1979). The filtered data for each block are listed in online Supplementary Material Tables S1–S3.

For consistency, the compiled zircon Hf isotopic data for magmatic zircons from the TTGs (online Supplementary Material Table S4; summarized in online Supplementary Material Fig. S1) were recalculated by adopting the same reference values: $^{176}Hf/^{177}Hf_{DM,0} = 0.28325$, $^{176}Lu/^{177}Hf_{DM,0} = 0.0384$ (Griffin *et al.* 2000), $^{176}Lu/^{177}Hf_{CHUR,0} = 0.0332$, $^{176}Hf/^{177}Hf_{CHUR,0} = 0.282772$ (Blichert-Toft & Albarède, 1997) and $\lambda = 1.867 \times 10^{-11}$ (Söderlund *et al.* 2004). Moreover, a $^{176}Lu/^{177}Hf$ value of 0.015 was adopted for the average continental crust (Griffin *et al.* 2002) to recalculate two-stage model ages (T_{DM2}). The recalculated values are listed in online Supplementary Material Table S4.

4. Results

4.a. Major and trace elements

In the An–Ab–Or geochemical classification diagram proposed by Barker & Arth (1976), the rocks classify as tonalitic, trondhjemitic and granodioritic (online Supplementary Material Fig. S2), clearly showing their affinity with the TTG suite of rocks. All of the samples plot in the metaluminous–peraluminous domains on the A/NK–A/CNK diagram (online Supplementary Material Fig. S3) and display a trondhjemitic trend in the K–Na–Ca plot (online Supplementary Material Fig. S2). In the three blocks, the 2.5 Ga TTGs exhibit similar A/NK and A/CNK values to those of the 2.7 Ga TTGs (online Supplementary Material Fig. S3), indicating that they are all Al-rich. In summary, major-element compositions of the TTG gneisses in the three blocks of the NCC share a number of similarities with Archaean TTG suites around the world (Martin *et al.* 2005, 2009). Generally speaking, the 2.5 Ga TTGs in the EB show higher Sr and Sr/Y than those
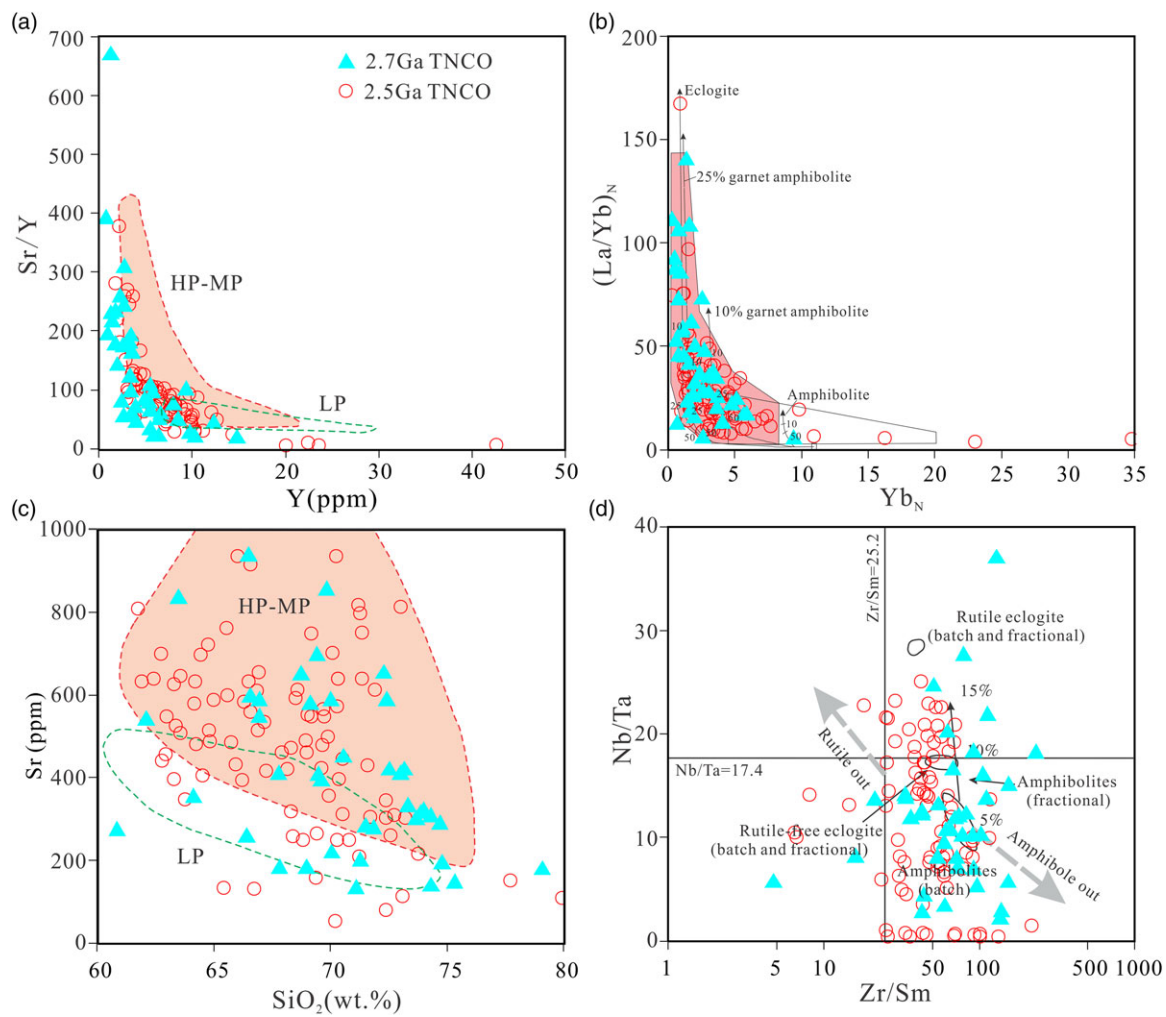
Fig. 2. (Colour online) (a) Sr/Y–Y, (b) (La/Yb)$_N$–Yb$_N$, (c) Sr–SiO$_2$ and (d) Nb/Ta–Zr/Sm diagrams for the TTG gneisses from the TNCO of the NCC (melting curves are from Drummond & Defant, 1990; HP, MP and LP TTGs are from Moyen, 2011). Note that the sample (10HXL-01) with remarkably high Sr/Y and two samples (12ZHF-02 and 12ZHF-04) with extremely high Nb/Ta ratios are not shown in (a) and (d), respectively.

of the TNCO and WB, while the 2.7 Ga TTGs in the EB show lower Sr, Sr/Y and ΔSr than those of the TNCO (Figs 2–5). Moreover, the two phases of TTGs in the EB show distinct Nb/Ta ratios while those TTGs in the TNCO possess similar Nb/Ta values (Figs 2, 3, 6). Detailed similarities and distinctions between the TTGs of different ages from the different blocks are described in the online Supplementary Material.

4.b. Hf isotopes of magmatic zircons

The Hf isotopes of magmatic zircons from the 2.5 and 2.7 Ga TTGs from the TNCO and EB are depicted in Figures 7 and 8, respectively. The T$_{DM2}$ histogram for the 2.5 Ga TTGs in the TNCO is consistent with a Gaussian normal distribution, with the T$_{DM2}$ ages varying between 2348 Ma and 3022 Ma and a single major peak at 2.69 Ga (Fig. 7a). The ε$_{Hf}$(t) values show relatively large ranges (+0.33 to +10.70, +5.28 on average; online Supplementary Material Table S4), mostly plotting between the crustal evolution curves of 2.5–3.0 Ga (Fig. 9a). In contrast, the 2.7 Ga TTGs from the TNCO show more complex Hf patterns than the 2.5 Ga TTGs in the T$_{DM2}$ histogram. The T$_{DM2}$ ages vary from 2680 Ma to 3424 Ma, with a predominant peak at 2.81 Ga and a subordinate peak at 3.06 Ga (Fig. 7b). The ε$_{Hf}$(t) values

(−3.85 to +7.87; online Supplementary Material Table S4) are relatively more negative than those of the 2.5 Ga TTGs.

The T$_{DM2}$ model ages of the 2.5 Ga TTGs from the EB are mainly concentrated between 2.5 Ga and 3.1 Ga, with a single peak at 2.74 Ga, and the ε$_{Hf}$(t) values range between −2.56 and +12.60 (average +4.59) (Fig. 8a; online Supplementary Material Table S4). However, the magmatic zircons of the 2.7 Ga TTGs from the EB show ε$_{Hf}$(t) values of −13.89 to +8.61 (average +3.76) and T$_{DM2}$ model ages mainly concentrating between 2.7 Ga and 3.2 Ga, with a major peak at 2.83 Ga and a subordinate peak at 2.94 Ga (Fig. 8b).

Limited Hf isotopic data from the WB are available, so the description of them is omitted here.

5. Discussion

5.a. Source material

It is commonly considered that TTG magmas were formed by partial melting of meta-basaltic rocks under a variety of conditions (e.g. Rapp & Watson, 1995; Martin *et al.* 2005). As different sources influence the compositions of TTG melts differently, the trace-element concentrations of juvenile TTGs can be employed to constrain their actual source compositions (Hoffman *et al.* 2011).
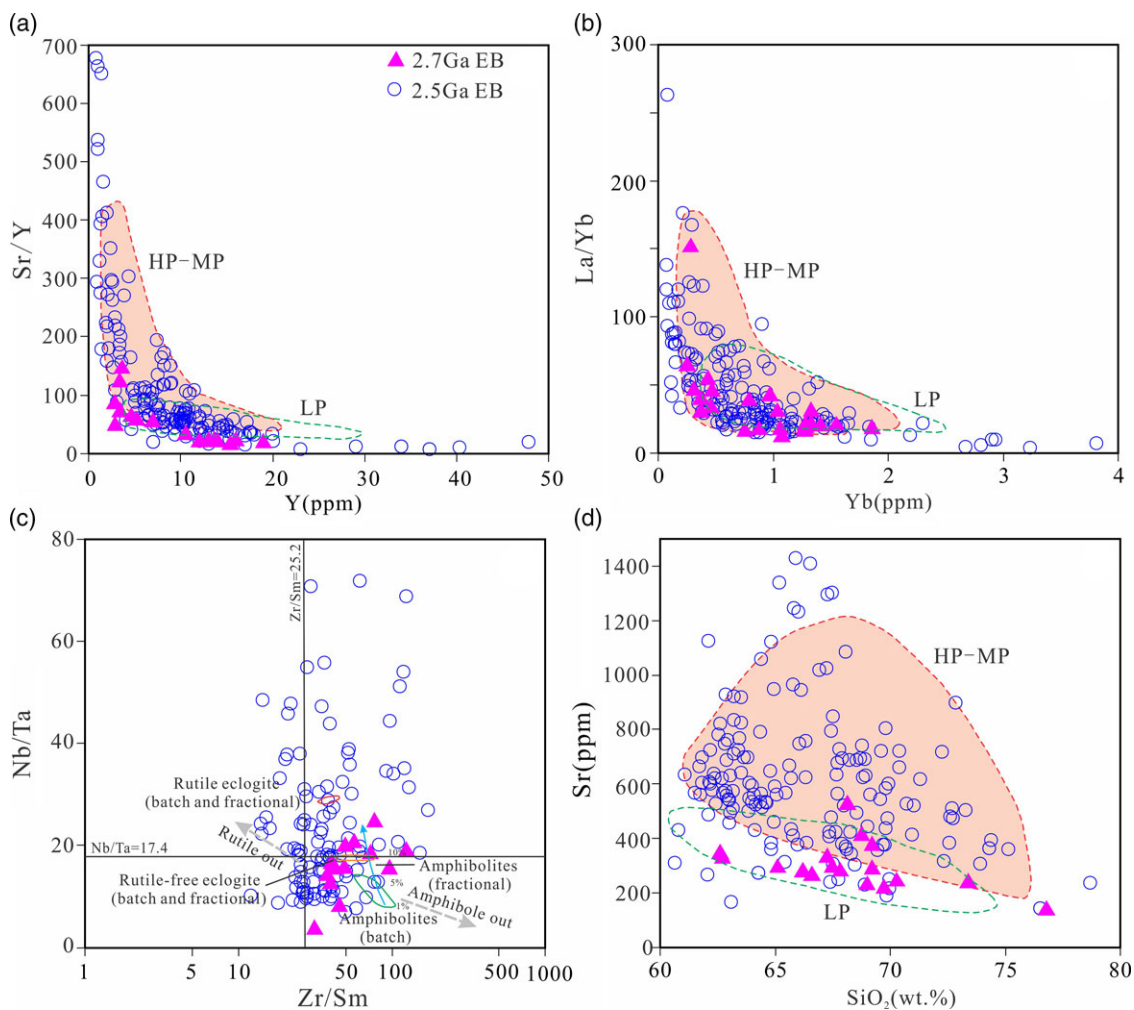
Fig. 3. (Colour online) (a) Sr/Y–Y, (b) (La/Yb)–Yb, (c) Nb/Ta–Zr/Sm and (d) Sr–SiO$_2$ diagrams for the TTG gneisses from the EB of the NCC (melting curves are from Drummond & Defant, 1990; HP, MP and LP TTGs are from Moyen, 2011).

For TTG magma, experimental studies show that the heavy rare earth elements (HREEs) are buffered mainly by garnet and/or amphibole, thus the HREE concentrations and patterns of the TTG melt can be used to speculate the stability of garnet/amphibole in the residue phase (Beard & Lofgren, 1991; Rapp *et al.* 1991, 1999, 2003; Foley *et al.* 2002, 2003; Moyen & Stevens, 2006). Generally, HREEs are strongly compatible within garnet, while medium rare earth elements (MREEs) are strongly enriched within amphibole (Rollinson, 1993). Therefore, the melting products derived from the melting of basaltic rocks in equilibrium with garnet residue should show very high fractionations between light rare earth elements (LREEs) and HREEs, while the counterpart equilibrated with amphibole residue would have a concave-upward normalized REE pattern (Rollinson, 1993). In addition, plagioclase is the main phase controlling Sr concentrations and Eu anomalies (Martin, 1987; Springer & Seck, 1997). Therefore, it is not hard to imagine that the melt would have high Sr contents and positive Eu anomalies if plagioclase breaks down during the melting process. Moreover, Yb$_N$–(La/Yb)$_N$ and Sr/Y–Y diagrams are generally used to discriminate the possible source of TTGs (Martin, 1986, 1987; Defant & Drummond, 1990; Moyen, 2009). The trace-element modelling results from Martin (1986) showed that low Yb and Y concentrations would result in high (La/Yb)$_N$ and Sr/Y ratios, which require garnet in the residue phase. Experimental studies

show that high field strength elements (HFSEs) and their ratios can reflect the partition behaviour of elements into different mineral phases (e.g. amphibole, rutile, ilmenite and titanite); therefore, they can be employed as good tracers for distinguishing different sources. It is commonly considered that rutile and amphibole play significant roles in buffering Nb and Ta, in which they possess opposite partition behaviour for Nb and Ta (Foley *et al.* 2002; Rapp *et al.* 2003). However, no consensus has been reached over which is the main mineral phase in the residue (Foley *et al.* 2002; Rapp *et al.* 2003; Xiong *et al.* 2005, 2006, 2009).

Based on a series of geochemical distinctions, Moyen (2011) divided the compiled TTG data from previously published literature into three subgroups: high-pressure (HP) TTG (20 %), medium-pressure (MP) TTG (60 %) and low-pressure (LP) TTG (20 %). The HP TTGs are characterized by high Al$_2$O$_3$, Na$_2$O and Sr but low Y, Yb, Ta and Nb; LP TTGs are enriched in HREEs and show low Sr, Sr/Y and La/Yb values, consistent with low-Al TTGs proposed by Barker (1979), and MP TTGs fall in between. On the basis of geochemical modelling results, Moyen (2011) proposed that these three subgroups of TTG magmas were generated at different melting depths and thus with different residue phases: HP TTGs were formed at pressures ≥ 20 kbar, with residues of garnet and rutile but without amphibole and plagioclase; MP TTGs were generated at pressures of ~15 kbar, with
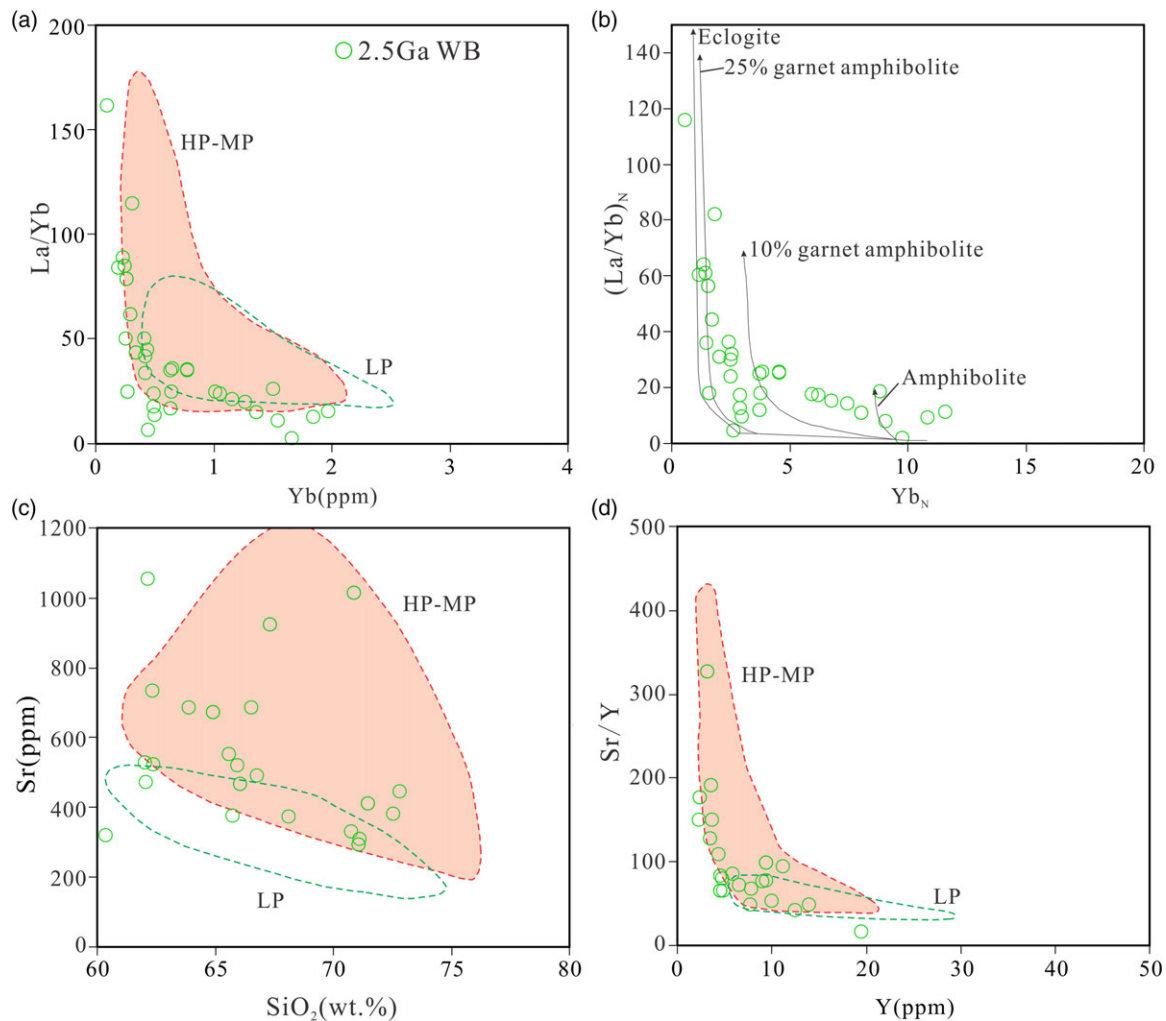
Fig. 4. (Colour online) (a) (La/Yb)–Yb, (b) (La/Yb)$_N$–Yb$_N$, (c) Sr–SiO$_2$ and (d) Sr/Y–Y diagrams for the TTG gneisses from the WB of the NCC (melting curves are from Drummond & Defant, 1990; HP, MP and LP TTGs are from Moyen, 2011).

amphibole and a significant amount of garnet but without rutile and plagioclase; and at ~10–12 kbar, LP TTGs were in equilibrium with residues of plagioclase–pyroxene–amphibole, with little garnet and no rutile.

5.a.1. TTGs from the EB

The 2.5 Ga TTGs in the EB are enriched in LREEs and depleted in HREEs, with very high Sr/Y and (La/Yb)$_N$ values (Fig. 3; online Supplementary Material Fig. S7; online Supplementary Material Table S1), indicating residues of garnet and/or amphibole (Beard & Lofgren, 1991; Rapp *et al.* 1991, 1999, 2003; Foley *et al.* 2002, 2003; Moyen & Stevens, 2006). The Y/Yb (mostly around 10.0, average 12.39) and (Ho/Yb)$_N$ ratios (0.40–2.47, average 1.23) for the 2.5 Ga TTGs in the EB indicate relatively flat HREE patterns and the residues of both garnet and amphibole. In addition, these rocks show high Sr contents (141–1431 ppm, 598 ppm on average) and nearly negligible Eu anomalies (Eu/Eu* = 1.44 on average), indicating that plagioclase does not exist in the residue phase. Their Nb/Ta ratios and the Nb/Ta–Zr/Sm diagram collectively indicate rutile is one of the residue phases for most of the samples. Additionally, the negative Nb, Ta and Ti anomalies (online Supplementary Material Fig. S7b) for the 2.5 Ga TTGs in EB can also be explained by rutile and amphibole residues (Xiong *et al.* 2005, 2006, 2009; Xiong, 2006).

Moreover, the 2.5 Ga TTGs in the EB resemble the HP–MP TTGs proposed by Moyen (2011) (Fig. 3), corroborating the residues inferred.

The 2.7 Ga TTGs in the EB are characterized by LREE enrichment and HREE depletion (online Supplementary Material Fig. S7c, d; online Supplementary Material Table S1), suggesting that garnet and/or amphibole exist in the residue (Beard & Lofgren, 1991; Rapp *et al.* 1991, 1999, 2003; Foley *et al.* 2002, 2003; Moyen & Stevens, 2006). The Y/Yb (7.30-14.87, average 10.63) and (Ho/Yb)$_N$ ratios (0.89–1.82, average 1.28) for the 2.7 Ga TTGs indicate relatively flat HREE patterns and the residues of both garnet and amphibole. These samples show negative to positive Eu anomalies, indicating that plagioclase exists in some samples but not in others. This can also provide an interpretation for the generally low Sr/Y ratios of the 2.7 Ga TTGs (Fig. 3; online Supplementary Material Table S1). Their Nb/Ta ratios (3.60–24.64) indicate, except for minor samples, that most samples do not contain rutile in the residue phase (Fig. 3c). Moreover, they are broadly similar to the LP TTGs of Moyen (2011), providing a further line of evidence for the above inference. Therefore, the 2.7 Ga TTGs in the EB are considered to have been formed at lower pressures than those of the 2.5 Ga TTGs, which is also demonstrated by the pressure-controlled ΔX parameters (Fig. 5).
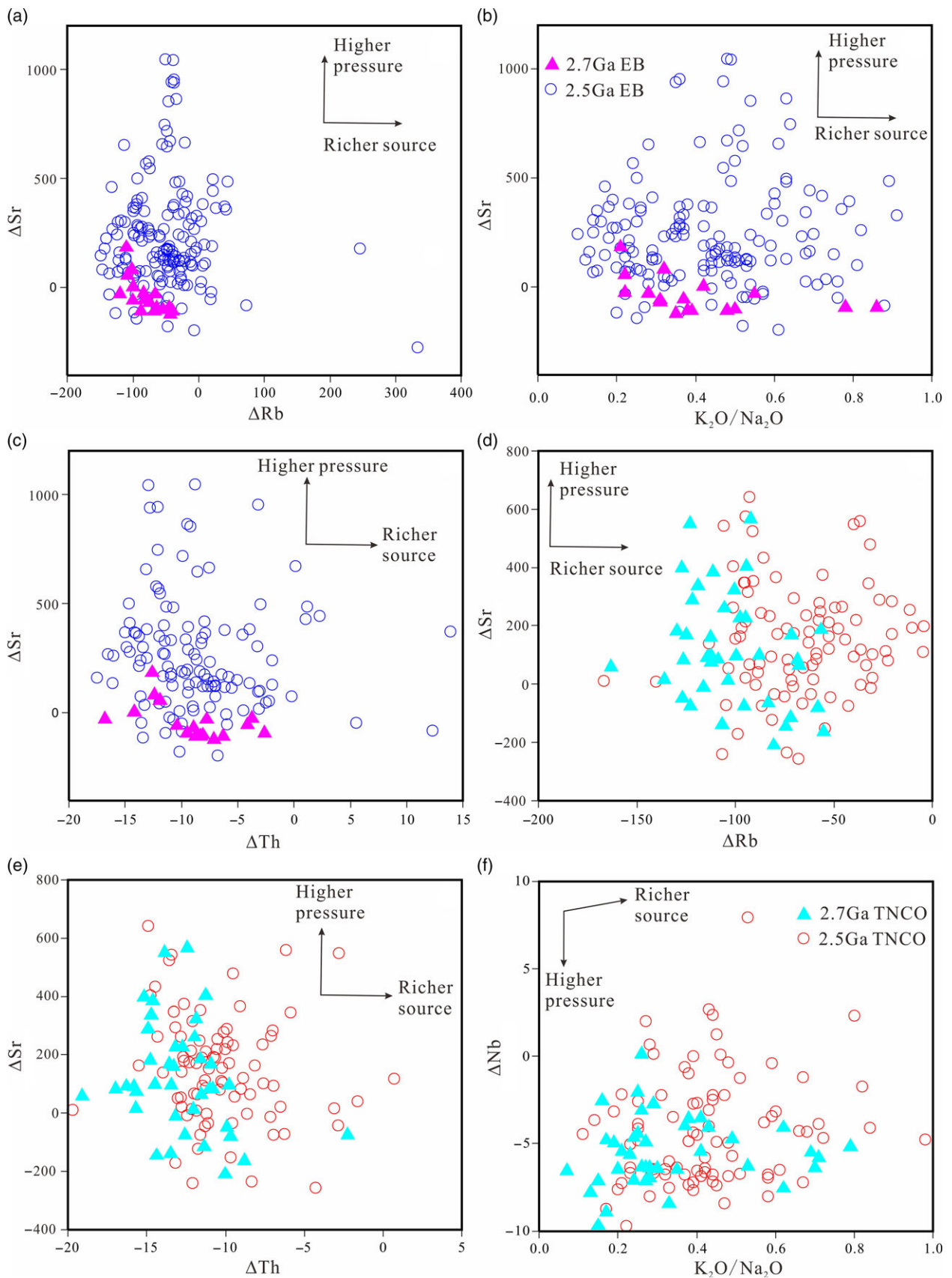
Fig. 5. (Colour online) Diagrams showing both source composition/enrichment and melting depth/pressure for the 2.5 and 2.7 Ga TTG gneisses from the (a–c) EB and (d–f) TNCO. (a) and (d) ΔSr versus ΔRb; (b) ΔSr versus K_2O/Na_2O; (c) and (e) ΔSr versus ΔTh; (f) ΔNb versus K_2O/Na_2O. For element X, ΔX = X − (aSiO$_2$ + b); constants of a and b and vectors to show the trends of higher pressures and richer sources are from Moyen *et al.* (2009).
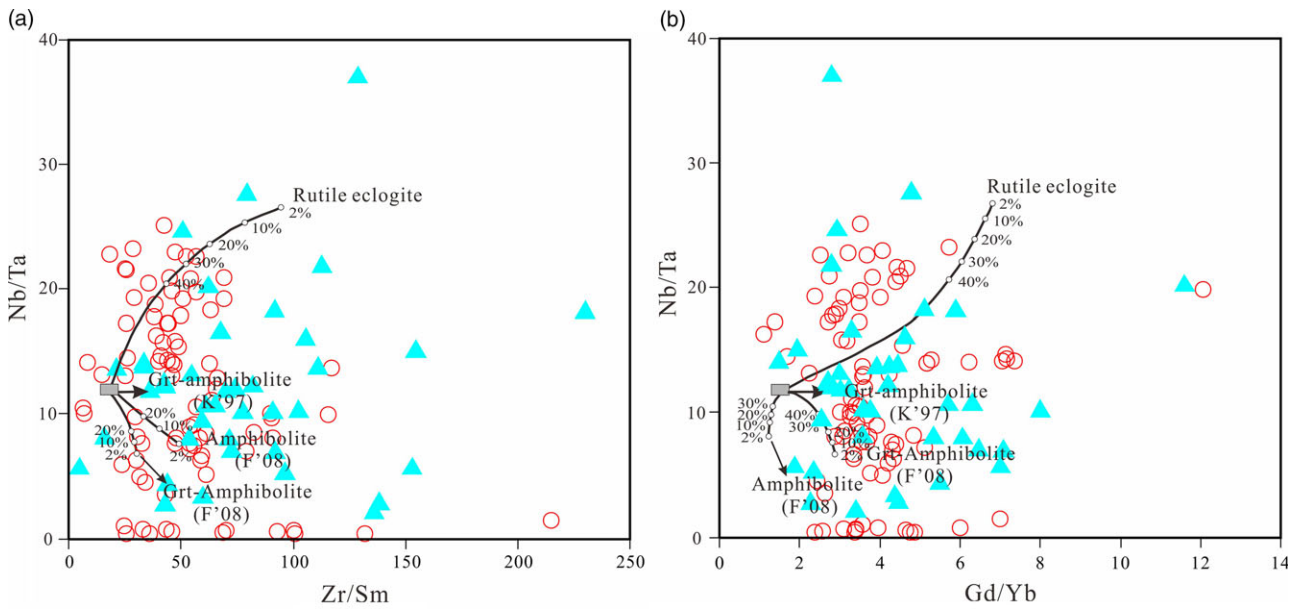
Fig. 6. (Colour online) Geochemical modelling ((a) Nb/Ta versus Zr/Sm and (b) Nb/Ta versus Gd/Yb) for the 2.5 and 2.7 Ga TTGs in the TNCO (melting curves are based on Shan *et al.* (2016)). Symbols are the same as those in Fig. 2. Note that two samples (12ZHF-02 and 12ZHF-04) with extremely high Nb/Ta ratios are not shown.

Fig. 7. (Colour online) Histograms showing zircon T_{DM2} model ages for the magmatic zircons from the (a) 2.5 Ga and (b) 2.7 Ga TTG gneisses in the TNCO of the NCC.
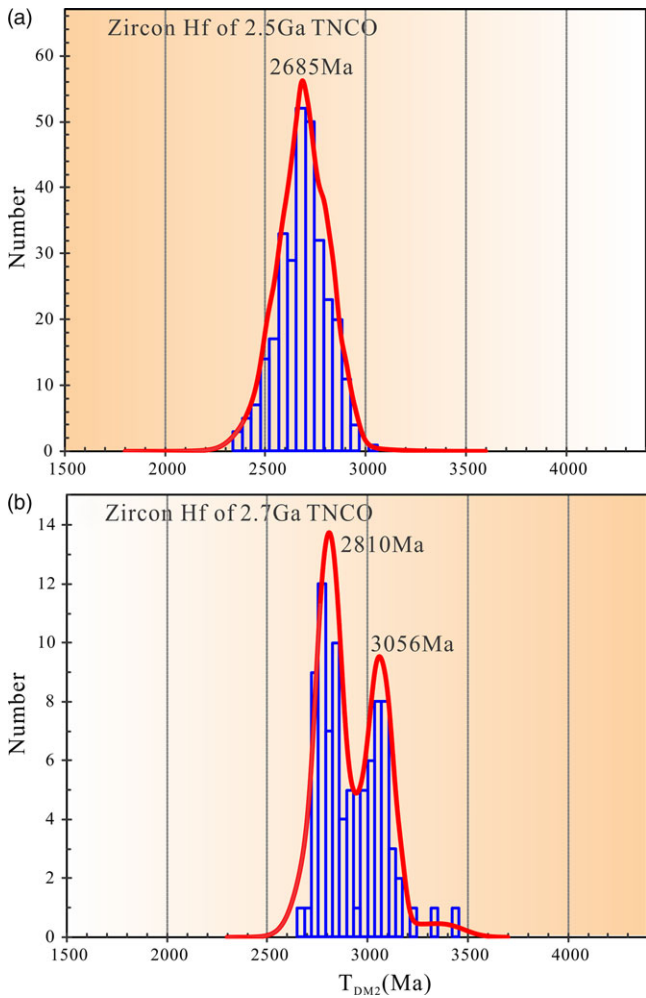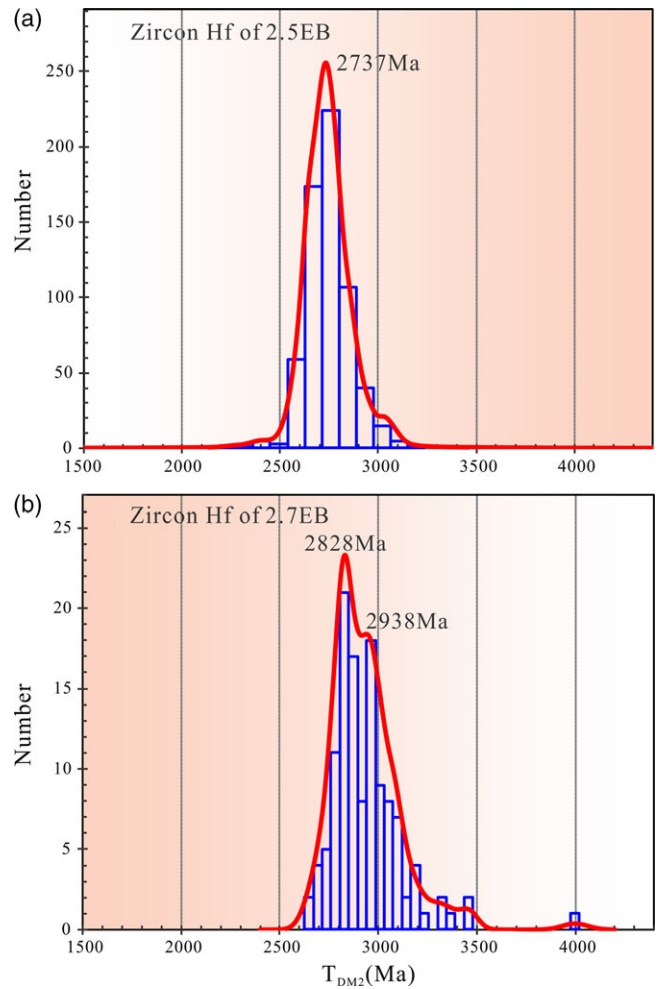
Fig. 8. (Colour online) Histograms showing zircon T_{DM2} model ages for the magmatic zircons from the (a) 2.5 Ga and (b) 2.7 Ga TTG gneisses in the EB of the NCC.

In summary, the 2.5 Ga TTGs in the EB are mainly formed by partial melting of rutile-bearing eclogite or garnet-amphibolite at higher pressure, while the 2.7 Ga TTGs were generated by partial melting of garnet-amphibolite or granulites at lower pressure.

5.a.2. TTGs from the TNCO

Similarly, the 2.5 and 2.7 Ga TTGs in the TNCO are also enriched in LREEs and depleted in HREEs (online Supplementary Material Fig. S5; online Supplementary Material Table S2), indicating garnet and/or amphibole residues (Beard & Lofgren, 1991; Rapp *et al.* 1991, 1999, 2003; Foley *et al.* 2002, 2003; Moyen & Stevens, 2006). The 2.5 and 2.7 Ga TTGs in the TNCO have Y/Yb ratios of 6.47–20.43 and 7.82–21.74, and $(Ho/Yb)_N$ ratios of 0.90–1.93 (average 1.27) and 0.60–1.88 (average 1.29), indicating relatively flat HREE patterns and the residues of both garnet and amphibole. Both the two phases of TTGs display high Sr contents and positive or negligible Eu anomalies, suggesting plagioclase breakdown during the process. Their Nb/Ta ratios range from 0.40–113 (average 13.49) and 2.04 to 37.00 (average 12.14), suggesting rutile existed in the residue phase of some, but not all, samples. This is also evidenced by the Nb/Ta–Zr/Sm diagram (Fig. 2d) that shows part of these two phases of the TTG samples plot in the garnet-amphibolite field and others in the eclogite domain, indicating that the 2.5 and 2.7 Ga TTGs in the TNCO were formed under conditions of garnet-amphibolite facies to eclogite facies. In the comparison diagram with the HP–MP–LP TTGs of Moyen (2011), such as Sr–SiO_2, $(La/Yb)_N$–Yb_N and Sr/Y–Y plots (Fig. 2a, b, c), the 2.5 and 2.7 Ga TTGs in the TNCO both plot in the HP–MP TTG domain and are strikingly distinct from LP TTGs, indicating formation conditions of garnet-amphibolite facies to eclogite facies. In addition, their Nb, Ta and Ti anomalies (online Supplementary Material Fig. S5b, d) can possibly be explained by residues of rutile and amphibole (Xiong *et al.* 2005, 2006, 2009; Xiong, 2006). Therefore, the source material of the 2.5 and 2.7 Ga TTGs in the TNCO is garnet-amphibolite or eclogite. This assertion can be further certified by the modelling results (Fig. 6), in which, except for two samples ZHF12-02 and ZHF12-04 with very high Nb/Ta ratios that are not shown in the modelling results, other samples of the 2.5 and 2.7 Ga TTGs in the TNCO can be well explained by polybaric melting of garnet-amphibolite or eclogite (Hoffman *et al.* 2011). But it is noteworthy that garnet-amphibolite predominates over eclogite in the source of the 2.7 Ga TTGs, while the two are nearly equal for the 2.5 Ga TTGs, suggesting generally deeper sources for the 2.5 Ga TTGs than those of the 2.7 Ga TTGs. Additionally, the source composition-controlled parameters (ΔRb, ΔTh and K_2O/Na_2O) shown on the horizontal axes of the diagrams (Fig. 5) indicate a more enriched source for the 2.5 Ga TTGs compared with that of the 2.7 Ga TTGs in the TNCO.

5.a.3. TTGs from the WB

The 2.5 Ga TTGs in the WB have high Sr contents and positive or negligible negative Eu anomalies, suggesting no plagioclase in the residue phase. The Y/Yb (7.09–31.00, average 13.01) and $(Ho/Yb)_N$ ratios (0.63–2.08, average 1.41) for the 2.5 Ga TTGs in WB indicate relatively flat HREE patterns (online Supplementary Material Fig. S9) and the residues of both garnet and amphibole. These TTGs show similarities to HP–MP TTGs in comparison diagrams, such as Sr–SiO_2, $(La/Yb)_N$–Yb_N and Sr/Y–Y (Fig. 4). As the number of Nb/Ta ratios is too small, it is not discernible whether there is rutile or not. Based on the above information, it can be inferred that

the source material of the 2.5 Ga TTGs in the WB was possibly garnet-amphibolite or eclogite, but this requires corroboration.

5.b. Tectonic setting

As to the tectonic setting of the TTGs, there is an ongoing controversy over whether they were formed by subduction, lower crustal thickening or delamination of an oceanic plateau (Smithies, 2000; Zegers & van Keken, 2001; Whalen *et al.* 2002; Condie, 2005; Martin *et al.* 2005; Bedard, 2006). Delamination of an oceanic plateau is not likely, because up to now there is no evidence of Archaean delamination in the NCC. According to experimental studies, partial melting of purely hydrous basalts would yield low Mg# values (< 45) and Ni contents (< 10 ppm), regardless of melting pressure (Rapp & Watson, 1995; Rapp *et al.* 1999; Wang *et al.* 2006). Melting of mafic rocks under a thickened lower crust will also have low Mg# values (< 45) and Cr (< 20–30 ppm) and Ni (< 20 ppm) contents (Atherton & Petford, 1993; Petford & Atherton, 1996; Wang *et al.* 2006). In contrast, melts from the partial melting of a subducting slab will generally have higher Mg# and Cr and Ni concentrations (Martin, 1999; Smithies, 2000; Martin & Moyen, 2002; Martin *et al.* 2005; Moyen, 2009), resulting from interaction of slab melts with the overlying mantle wedge (Rapp *et al.* 1999, 2010). In addition, TTG melts from slab melting and thickened lower crust are characterized by distinct isotopic features. For example, TTG melts from slab melting will be equivalent to modern adakites in most aspects. If formed in an oceanic arc, TTG melts will have juvenile initial Nd and Hf isotopes; if generated in a continental arc, they will possess a large range of initial Nd and Hf isotope values from juvenile to evolved. In contrast with slab melts, the melts from thickened lower crust will have evolved features of initial Nd and Hf isotopes. Based on the above distinctions, the tectonic settings of the two phases of TTGs from the three blocks will be discussed in detail as follows.

5.b.1. TTGs from the EB

Compared with those magmas that originated from pure partial melting of thickened lower crust, the 2.5 Ga TTG gneisses in the EB show relatively high MgO contents, Mg# and Cr and Ni concentrations (online Supplementary Material Table S1), similar to TTG melts produced by slab melting (online Supplementary Material Fig. S6; Martin, 1999; Smithies, 2000; Martin & Moyen, 2002; Martin *et al.* 2005; Moyen, 2009) and show distinct differences from pure partial melting of hydrous basalts (Rapp & Watson, 1995; Rapp *et al.* 1999) and melts from thickened lower crust (Atherton & Petford, 1993; Petford & Atherton, 1996; Wang *et al.* 2006). Therefore, they are identical to many ~2.5 Ga TTGs worldwide (e.g. Martin & Moyen, 2002; Martin *et al.* 2005). Given these observations, the 2.5 Ga TTG gneisses in the EB are more likely to have formed by partial melting of subducted oceanic crust, followed by interaction with the overlying mantle wedge during ascent. The above inferences are also confirmed by the Hf isotopic data for magmatic zircons in Figure 8a, in which the initial Hf isotopes of the 2.5 Ga TTGs are characterized by juvenile to evolved signatures.

Compared with the 2.5 Ga TTGs in the EB, the 2.7 Ga TTGs show lower MgO contents (average 1.39 wt %), Mg# (average 43.71), Cr (average 14.93 ppm) and Ni (average 12.60 ppm) concentrations (online Supplementary Material Table S1), identical to adakites generated by thickened lower crust (online Supplementary Material Fig. S6; e.g. Martin & Moyen, 2002; Martin *et al.* 2005; Wang *et al.* 2006)

but distinct from TTGs formed by slab melting (Martin, 1999; Smithies, 2000; Martin & Moyen, 2002; Martin *et al.* 2005; Moyen, 2009). Their T_{DM2} model ages are concentrated between 2.9 Ga and 3.2 Ga with minor ages between 2.7 Ga and 2.8 Ga, which are diagnostic of initial Hf isotopes of thickened lower crust (Fig. 8b). Given these observations, the 2.7 Ga TTG gneisses in the EB are more likely to have formed by partial melting of thickened lower crust, without interaction with the overlying mantle wedge during ascent.

5.b.2. TTGs from the TNCO

Similar to the 2.5 Ga TTGs in the EB, the 2.5 Ga TTGs in the TNCO have high Mg# and Cr and Ni concentrations (online Supplementary Material Table S2), identical to many worldwide TTGs at ~2.5 Ga and TTGs generated by slab melting (online Supplementary Material Fig. S4; e.g. Martin, 1999; Smithies, 2000; Martin & Moyen, 2002; Martin *et al.* 2005; Moyen, 2009). Furthermore, the T_{DM2} histogram shows that nearly half of the T_{DM2} ages are concentrated between 2.5 Ga and 2.7 Ga and another half between 2.7 Ga and 2.9 Ga, representative of juvenile to evolved characteristics (Fig. 7a). Therefore, given these observations, the 2.5 Ga TTG gneisses in the TNCO are more likely to have formed by partial melting of subducted oceanic crust, followed by interaction with the overlying mantle wedge during ascent.

In contrast, the 2.7 Ga TTGs in the TNCO have relatively high Mg# but low Cr and Ni contents (online Supplementary Material Table S2), which seems to contradict each other, as high Mg# values indicate possible slab melting while relatively low Cr and Ni might be attributed to a lower crust origin. However, Getsinger *et al.* (2009) proposed that felsic melts would not be emplaced and condensed right away following their formation. Therefore, during their stay in the magma chamber, interaction would possibly occur between them and the melt residue in the lower crust, which would increase the Mg# of the melts, but it is hard to increase the Cr and Ni contents. Therefore, the most feasible explanation is a lower crust origin. Moreover, the isotopic evidence also supports this interpretation. The T_{DM2} model ages mostly range from 2.9 Ga to 3.2 Ga with minor ages lying between 2.7 Ga and 2.9 Ga, indicating evolved characteristics. Therefore, it is proposed that the 2.7 Ga TTGs in the TNCO were formed by lower crustal genesis.

5.b.3. TTGs from the WB

Different from both the EB and the TNCO, the WB has yet to yield any exposed 2.7 Ga TTGs. The 2.5 Ga TTGs in the WB have high Mg# and Cr and Ni concentrations (online Supplementary Material Table S3), identical to adakites generated by slab melting (online Supplementary Material Fig. S8; e.g. Martin & Moyen, 2002; Martin *et al.* 2005; Wang *et al.* 2006). Given these observations, the 2.5 Ga TTG gneisses in the WB are more likely to have formed by partial melting of subducted oceanic crust, followed by interaction with the overlying mantle wedge during ascent. Nonetheless, this interpretation requires more data (e.g. isotopes) for confirmation.

5.c. Constraints on the crustal growth and evolution in the NCC

5.c.1. Magma nature of the ~2.5 Ga and ~2.7 Ga TTGs

Regarding the definition of crustal growth, there are several viewpoints. Some researchers consider that if the $\varepsilon_{Hf}(t)$ of zircons is ≥ 0.75 times the Hf of the depleted mantle (DM) curve, they can be identified as recording 'crustal growth'

(Belousova *et al.* 2010). In addition, the difference between the Hf model ages of magmatic zircons and U–Pb ages is referred to as the crustal residence time (CRT; Griffin *et al.* 2006; Belousova *et al.* 2009). Therefore, a short CRT (< 200 Myr) means these rocks were derived from the DM or remelting of newly formed crust, which is called crustal growth by other scholars (Belousova *et al.* 2010; Hawkesworth *et al.* 2010). The CRT of some zircons is > 200 Myr, leaving the rest < 200 Myr, suggesting that the 2.5 Ga TTG magmas of the whole NCC derived from both older crustal reworking and juvenile crustal growth (Fig. 9c). On the $\varepsilon_{Hf}(t)$ versus age diagram (Fig. 9a), some $\varepsilon_{Hf}(t)$ values of the 2.5 Ga TTGs from the three blocks plot near the DM evolution curve and above the 0.75 * ε_{Hf} of DM curve, with most data points below this curve, demonstrating that the 2.5 Ga TTG magmas were mainly formed by remelting of older crust with a subordinate amount from juvenile crust. On the whole, most of these $\varepsilon_{Hf}(t)$ values plot between the crustal evolution curves of 2.5–3.0 Ga (Fig. 9a); therefore, it can be inferred that these crustal materials were extracted from the mantle during 3.0–2.5 Ga, or even older. A T_{DM2} model age histogram for all the 2.5 Ga data shows a major peak concentrated at 2.7–2.8 Ga (Fig. 9b), implying the 2.5 Ga TTG magmas in the NCC were related mainly with reworking of 2.8–2.7 Ga crust and relatively less with juvenile crustal growth during 2.6–2.5 Ga.

Generally, the 2.5 Ga TTGs from the EB and the TNCO show similar $\varepsilon_{Hf}(t)$ ranges, whereas those from the WB commonly have lower values on the whole (Fig. 9a), resulting in older T_{DM2} ages and a longer CRT for the 2.5 Ga TTGs in the WB (Fig. 9b, c, d). On one hand, this suggests that some of the 2.5 Ga TTGs from the WB were derived from reworking of relatively much older continental crust. More significantly, on the other hand, it implies that old continental crust as old as 3.5 Ga might exist in the WB, which has significant implications for the crustal evolution of the WB in early times.

Similar to the 2.5 Ga TTG magmas, a portion of the CRT values of the 2.7 Ga TTGs are < 200 Myr while the remaining are > 200 Myr, indicating that both crustal reworking and juvenile crustal growth were involved in the generation of the 2.7 Ga TTGs (Fig. 9g, h). Moreover, some data are distributed on or near the DM evolution curve and above the 0.75 * ε_{Hf} of DM, with T_{DM2} ages nearly equal or very close to the magmatic crystallization ages (Fig. 9e, f), thus representing juvenile crustal growth. However, most $\varepsilon_{Hf}(t)$ values plot far away from the DM evolution curve and below the 0.75 * ε_{Hf} of DM, with T_{DM2} model ages (2.9–3.4/3.5 Ga) much older than their magmatic crystallization ages (Fig. 9e, f), indicating that they were derived from the remelting of 3.4/3.5–2.9 Ga crust. In addition, their $\varepsilon_{Hf}(t)$ values plot between the crustal evolution curves of 2.7–3.5 Ga (Fig. 9e), representative of the time of mantle extraction of crustal material in the NCC. As a whole, the 2.7 Ga TTGs in the EB and TNCO show similar Hf isotopic features, implying a consistent or similar magmatic evolution for the EB and TNCO at 2.7 Ga, which is also the case with the 2.5 Ga EB and TNCO.

In summary, both the *c.* 2.5 Ga and *c.* 2.7 Ga TTG magmas can be interpreted as dual events involved with both crustal growth and crustal reworking, and both of them are dominated by crustal reworking over juvenile crustal growth. Additionally, the EB and TNCO might have witnessed a consistent or similar magmatic evolution at 2.7 Ga and 2.5 Ga, and some of the 2.5 Ga TTGs from the WB were derived from reworking of relatively much older continental crust.
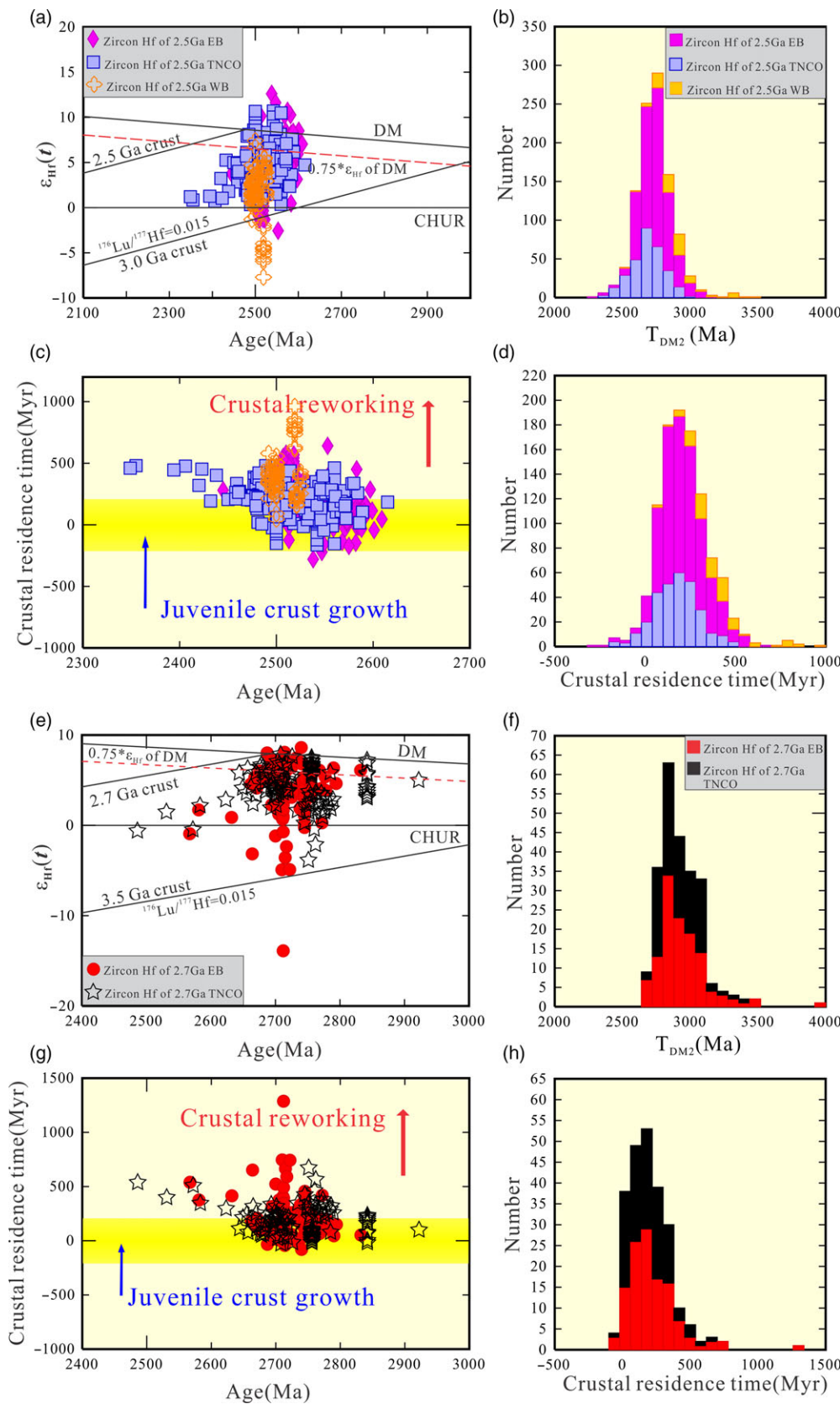
Fig. 9. (Colour online) (a, e) $\varepsilon_{Hf}(t)$ versus $^{207}Pb/^{206}Pb$ age (Ma), (b, f) histograms showing zircon T_{DM2} model ages, (c, g) crustal residence time (Myr) versus $^{207}Pb/^{206}Pb$ age (Ma) and (d, h) histograms showing crustal residence time (Myr) for the magmatic zircons from the (a–d) 2.5 Ga and (e–h) 2.7 Ga TTG gneisses of the NCC. DM – depleted mantle; CHUR – chondritic uniform reservoir.

5.c.2. Neoarchaean crustal evolution of the three blocks and the whole NCC

As there are only limited data from the WB, the discussions here focus on the TNCO and EB. Zircon Hf isotopes from the TNCO show that the T_{DM2} model ages mainly range from 2.5 Ga to 3.1 Ga with a peak at 2.7–2.8 Ga (Fig. 10a), and $\varepsilon_{Hf}(t)$ values mostly plot between the crustal evolution curves of 2.5–3.1 Ga (Fig. 10b). All these data suggest that crustal growth in the TNCO mainly took
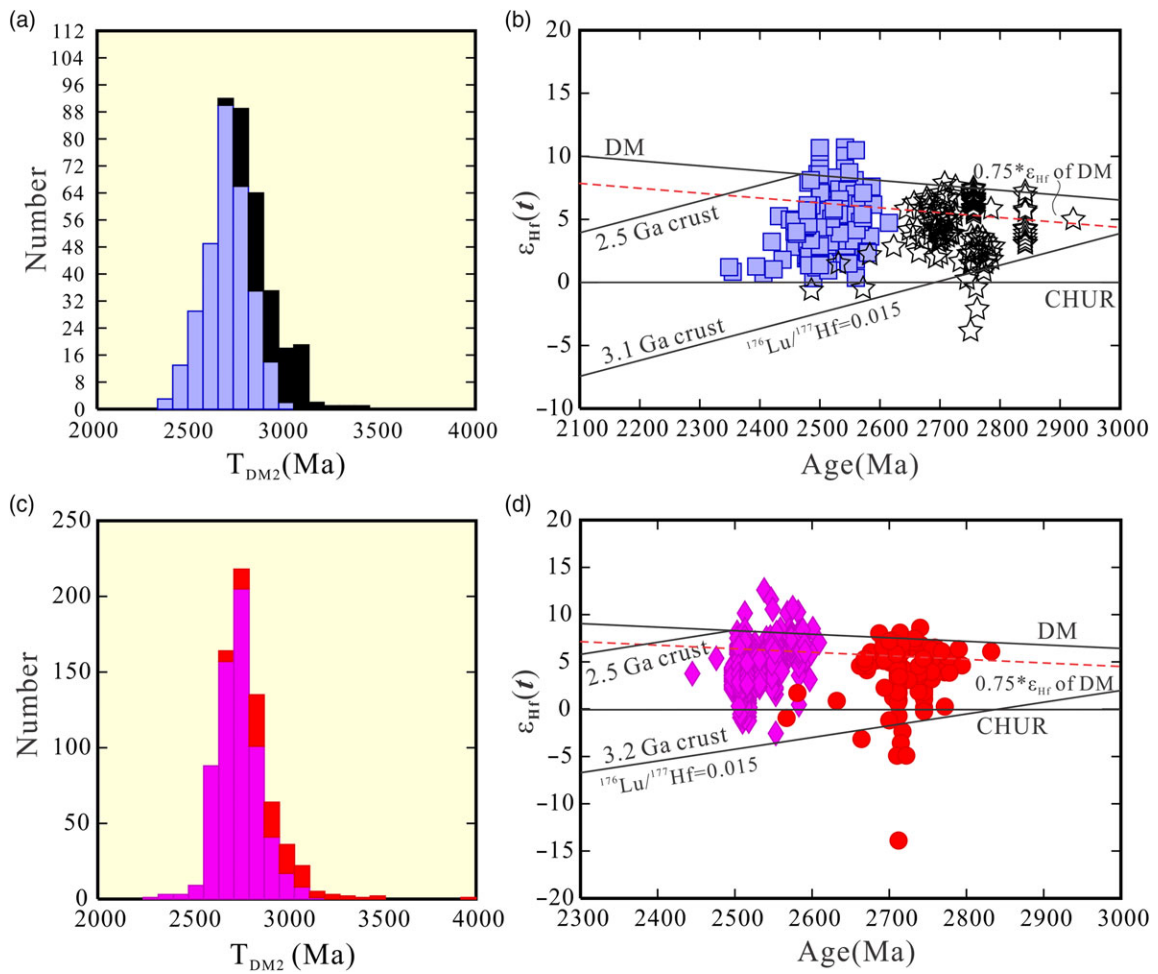
Fig. 10. (Colour online) (a, c) Histograms showing zircon T_{DM2} model ages and (b, d) $\varepsilon_{Hf}(t)$ versus $^{207}Pb/^{206}Pb$ age (Ma) for the magmatic zircons from the TTG gneisses in the (a, b) TNCO and (c, d) EB of the NCC. Symbols are the same as those in Figure 9. DM – depleted mantle; CHUR – chondritic uniform reservoir.
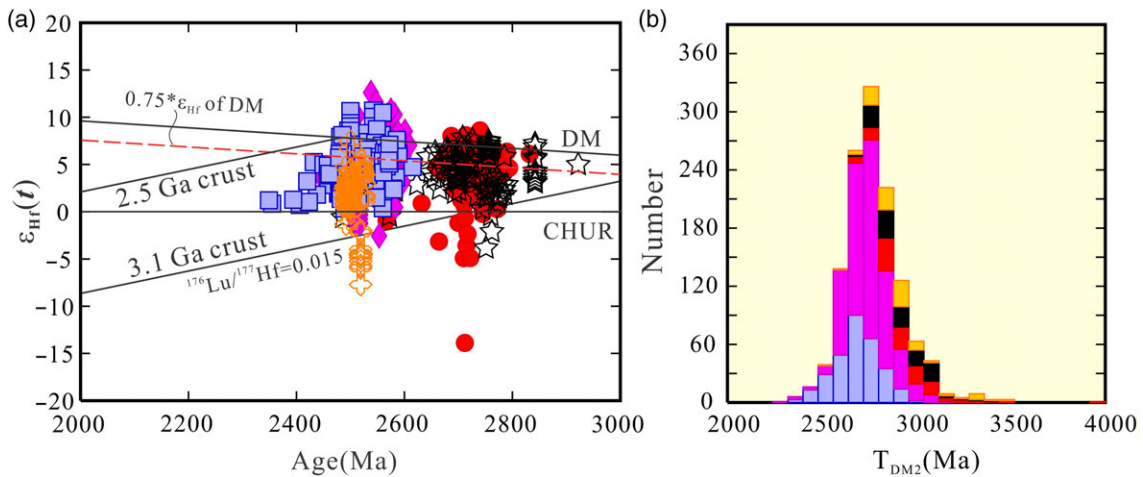

Fig. 11. (Colour online) (a) $\varepsilon_{Hf}(t)$ versus $^{207}Pb/^{206}Pb$ age (Ma) and (b) histograms showing zircon T_{DM2} model ages for the magmatic zircons from the TTG gneisses of the NCC. Symbols are the same as those in Figure 9. DM – depleted mantle; CHUR – chondritic uniform reservoir.

place during 3.1–2.5 Ga, with the dominant growth period at 2.8–2.7 Ga. Similarly, the Hf isotopic data for the EB display a main range of T_{DM2} model ages of 2.5 Ga to 3.2 Ga with a peak at 2.7–2.9 Ga (Fig. 10c). Most of the $\varepsilon_{Hf}(t)$ data points lie between the crustal evolution curves of 2.5–3.2 Ga (Fig. 10d). These data suggest that a

crustal growth event existed during 3.2–2.5 Ga and was concentrated between 2.9 Ga and 2.7 Ga. Finally, all the data were plotted on a $\varepsilon_{Hf}(t)$ versus age diagram and T_{DM2} model age histogram (Fig. 11). The plots show that the T_{DM2} model ages are mainly concentrated between 2.7 and 2.9 Ga and subordinately concentrated

at ~2.5 Ga and 3.0/3.1 Ga (Fig. 11b), indicating that the whole NCC witnessed a major crustal growth event at 2.9–2.7 Ga and a minor growth at ~3.0/3.1 Ga and ~2.5 Ga. The $\varepsilon_{Hf}(t)$ values display a relatively large range that mainly plot between the crustal evolution curves of 2.5–3.2 Ga, also indicating a mantle extraction event occurred at 3.1–2.5 Ga (Fig. 11a).

6. Conclusions

(1) The source material of the 2.5 Ga TTGs in the EB is rutile-bearing eclogite or garnet-amphibolite at higher pressure, possibly formed by partial melting of a subducting slab, while the 2.7 Ga TTGs from the EB were derived from melting of garnet-amphibolite or granulite at lower pressure, perhaps at the base of thickened lower crust.

(2) The 2.5 and 2.7 Ga TTGs from the TNCO were formed under garnet-amphibolite- to eclogite-facies conditions by partial melting of a subducting slab and thickened lower crust, respectively, with a deeper and more enriched source for the former compared with that of the latter; the 2.5 Ga TTGs from the WB were generated by melting of a subducting slab with source materials of garnet-amphibolite or eclogite.

(3) Both the *c.* 2.5 Ga and *c.* 2.7 Ga TTG magmas can be interpreted as dual events involved with both crustal growth and crustal reworking, and both of them are predominated by crustal reworking over juvenile crustal growth. Additionally, the EB and TNCO might have witnessed consistent or similar magmatic evolution at 2.7 Ga and 2.5 Ga; some of the 2.5 Ga TTGs from the WB were derived from reworking of relatively much older continental crust.

(4) The major crustal growth in the TNCO was concentrated between 2.8 Ga and 2.7 Ga, while that for the EB occurred during 2.9–2.7 Ga. The whole NCC witnessed a major crustal growth event at 2.9–2.7 Ga and a minor growth at 3.0/3.1 Ga and ~2.5 Ga.

Supplementary material. To view supplementary material for this article, please visit https://doi.org/10.1017/S0016756820000618

References

Arndt NT and Goldstein SL (1989) An open boundary between lower continental crust and mantle: its role in crust formation and crustal recycling. *Tectonophysics* **161**, 201–12.

Arth JG and Hanson GN (1972) Quartz diorites derived by partial melting of eclogite or amphibolite at mantle depths. *Contributions to Mineralogy and Petrology* **37**, 161–74.

Atherton MP and Petford N (1993) Generation of sodium-rich magmas from newly underplated basaltic crust. *Nature* **362**, 144–6.

Barker F (1979) Trondhjemite: definition, environment and hypotheses of origin. In *Trondhjemites, Dacites and Related Rocks* (ed. F Barker), pp. 1–12. Amsterdam: Elsevier.

Barker F and Arth JG (1976) Generation of trondhjemitic-tonalitic liquids and Archean bimodal trondhjemite-basalt suites. *Geology* **4**, 596–600.

Beard JS and Lofgren GE (1991) Dehydration melting and water-saturated melting of basaltic and andesitic greenstones and amphibolites at 1, 3, and 6.9 kb. *Journal of Petrology* **32**, 365–401.

Bedard JH (2006) A catalytic delamination-driven model for coupled genesis of Archean crust and sub-continental lithospheric mantle. *Geochimica et Cosmochimica Acta* **70**, 1188–214.

Belousova EA, Kostitsyn YA, Griffin WL, Begg GC, O'Reilly SY and Pearson NJ (2010) The growth of the continental crust: constraints from zircon Hf-isotope data. *Lithos* **119**, 457–66.

Belousova EA, Reid AJ, Griffin WL and O'Reilly SY (2009) Rejuvenation vs. recycling of Archean crust in the Gawler Craton, South Australia: evidence from U–Pb and Hf isotopes in detrital zircon. *Lithos* **113**, 570–82.

Blichert-Toft J and Albarède F (1997) The Lu–Hf isotope geochemistry of chondrites and the evolution of the mantle-crust system. *Earth and Planetary Science Letters* **148**, 243–58.

Condie KC (2005) TTGs and adakites: are they both slab melts? *Lithos* **80**, 33–44.

Defant MJ and Drummond MS (1990) Derivation of some modern arc magmas by melting of young subducted lithosphere. *Nature* **347**, 662–5.

Drummond MS and Defant MJ (1990) A model for trondhjemite-tonalite-dacite genesis and crustal growth via slab melting: Archean to modern comparisons. *Journal of Geophysical Research: Solid Earth* **95**, 21503–21.

Foley S, Buhre S and Jacob DE (2003) Evolution of the Archaean crust by delamination and shallow subduction. *Nature* **421**, 249–52.

Foley SF, Tiepolo M and Vannucci R (2002) Growth of early continental crust controlled by melting of amphibolite in subduction zones. *Nature* **417**, 837–40.

Getsinger A, Rushmer T, Jackson MD and Baker D (2009) Generating high Mg-numbers and chemical diversity in tonalite-trondhjemite-granodiorite (TTG) magmas during melting and melt segregation in the continental crust. *Journal of Petrology* **50**, 1935–54.

Glikson AY (1979) Early Precambrian tonalite-trondhjemite sialic nuclei. *Earth Science Reviews* **15**, 1–73.

Griffin WL, Belousova EA, Walters SG and O'Reilly SY (2006) Archaean and Proterozoic crustal evolution in the Eastern Succession of the Mt Isa district, Australia: U–Pb and Hf-isotope studies of detrital zircons. *Australian Journal of Earth Sciences* **53**, 125–49.

Griffin WL, Pearson NJ, Belousova E, Jackson SE, Achterbergh E, Suzanne YO and Shee SR (2000) The Hf isotope composition of cratonic mantle: LAM-MC-ICPMS analysis of zircon megacrysts in kimberlites. *Geochimica et Cosmochimica Acta* **64**, 133–47.

Griffin W, Wang X, Jackson S, Pearson N, O'Reilly SY, Xu X and Zhou X (2002) Zircon chemistry and magma mixing, SE China: in-situ analysis of Hf isotopes, Tonglu and Pingtan igneous complexes. *Lithos* **61**, 237–69.

Guo JH, Sun M, Chen FK and Zhai MG (2005) Sm–Nd and SHRIMP U–Pb zircon geochronology of high-pressure granulites in the Sanggan area, North China Craton: timing of Paleoproterozoic continental collision. *Journal of Asian Earth Sciences* **24**, 629–42.

Guo JH and Zhai MG (2001) Sm–Nd age dating of high-pressure granulites and amphibolites from the Sanggan area, North China Craton. *Chinese Science Bulletin* **46**, 106–10.

Hawkesworth CJ, Dhuime B, Pietranik AB, Cawood PA, Kemp AIS and Storey CD (2010) The generation and evolution of the continental crust. *Journal of the Geological Society, London* **167**, 229–48.

Hoffmann JE, Carsten M, Næraa T, Rosing MT, Herwartz D, Garbe-Schonberg D and Svahnberg H (2011) Mechanisms of Archean crust formation inferred from high-precision HFSE systematics in TTGs. *Geochimica et Cosmochimica Acta* **75**, 4178.

Jahn BM, Auvray B, Cornichet J, Bai YL, Shen QH and Liu DY (1987) 3.5 Ga old amphibolites from eastern Hebei Province, China: field occurrence, petrography, Sm–Nd isochron age and REE geochemistry. *Precambrian Research* **34**, 311–46.

Jahn BM, Auvray B, Shen QH, Liu DY, Zhang ZQ, Dong YJ, Ye XJ, Zhang QZ, Cornichet J and Mace J (1988) Archean crustal evolution in China: the Taishan complex, and evidence for juvenile crustal addition from long-term depleted mantle. *Precambrian Research* **38**, 381–403.

Kröner A (1991) Tectonic evolution in the Archaean and Proterozoic. *Tectonophysics* **187**, 393–410.

Kröner A and Layer PW (1992) Crust formation and plate motion on the early Archean. *Science* **256**, 1405–11.

Kröner A, Wilde SA, Li JH and Wang KY (2005) Age and evolution of a late Archean to Paleoproterozoic upper to lower crustal section in the Wutaishan/Hengshan/Fuping terrain of northern China. *Journal of Asian Earth Sciences* **24**, 577–95.

Kröner A, Wilde SA, Zhao GC, O'Brien PJ, Sun M, Liu DY, Wan YS, Liu S and Guo JH (2006) Zircon geochronology and metamorphic evolution of mafic dykes in the Hengshan complex of northern China: evidence for late Paleoproterozoic extension and subsequent high-pressure metamorphism in the North China Craton. *Precambrian Research* **146**, 45–67.

Kusky TM (2011) Geophysical and geological tests of tectonic models of the North China Craton. *Gondwana Research* **20**, 26–35.

Kusky TM and Li JH (2003) Paleoproterozoic tectonic evolution of the North China Craton. *Journal of Asian Earth Sciences* **22**, 383–97.

Kusky T, Li J and Santosh M (2007) The Paleoproterozoic North Hebei Orogen: North China craton's collisional suture with the Columbia supercontinent. *Gondwana Research* **12**, 4–28.

Li XP, Yang ZY, Zhao GC, Grapes R and Guo JH (2011a) Geochronology of khondalite-series rocks of the Jining complex: confirmation of depositional age and tectonometamorphic evolution of the North China Craton. *International Geology Review* **53**, 1194–211.

Li SZ and Zhao GC (2007) SHRIMP U–Pb zircon geochronology of the Liaoji granitoids: constraints on the evolution of the Paleoproterozoic Jiao-Liao-Ji belt in the Eastern Block of the North China Craton. *Precambrian Research* **158**, 1–16.

Li SZ, Zhao GC, Santosh M, Liu X and Dai LM (2011b) Palaeoproterozoic tectonothermal evolution and deep crustal processes in the Jiao-Liao-Ji Belt, North China Craton: a review. *Geological Journal* **46**, 525–43.

Li SZ, Zhao GC, Sun M, Han ZZ, Luo Y, Hao DF and Xia XP (2005) Deformation history of the Paleoproterozoic Liaohe assemblage in the eastern block of the North China Craton. *Journal of Asian Earth Sciences* **24**, 659–74.

Li Z, Zhao GC, Sun M, Han ZZ, Zhao GT and Hao DF (2006) Are the South and North Liaohe Groups of the North China Craton different exotic terranes? Nd isotope constraints. *Gondwana Research* **9**, 198–208.

Li SZ, Zhao GC, Sun M, Wu FY, Liu JZ, Hao DF, Han Z and Luo Y (2004) Mesozoic, not Paleoproterozoic SHRIMP U–Pb zircon ages of two Liaoji granites, Eastern Block, North China Craton. *International Geology Review* **46**, 162–76.

Liu DY, Nutman AP, Compston W, Wu JS and Shen QH (1992) Remnants of ≥3800 Ma crust in the Chinese part of the Sino-Korean craton. *Geology* **20**, 339–42.

Liu SW, Zhao GC, Wilde SA, Shu GM, Sun M, Li QG, Tian W and Zhang J (2006) Th–U–Pb monazite geochronology of the Lvliang and Wutai complex: constraints on the tectonothermal evolution of the Trans-North China Orogen. *Precambrian Research* **148**, 205–24.

Lu LZ, Xu XC and Liu FL (1996) *Early Precambrian Khondalites in Northern China.* Changchun: Changchun Press, 276 pp.

Luo Y, Sun M, Zhao GC, Ayers JC, Li SZ, Xia XP and Zhang JH (2008) A comparison of U–Pb and Hf isotopic compositions of detrital zircons from the North and South Liaohe Group: constraints on the evolution of the Jiao-Liao-Ji Belt, North China Craton. *Precambrian Research* **163**, 279–306.

Martin H (1986) Effect of steeper Archean geothermal gradient on geochemistry of subduction-zone magmas. *Geology* **14**, 753–6.

Martin H (1987) Petrogenesis of Archaean trondhjemites, tonalites, and granodiorites from eastern Finland: major and trace element geochemistry. *Journal of Petrology* **28**, 921–53.

Martin H (1999) Adakitic magmas: modern analogues of Archaean granitoids. *Lithos* **46**, 411–29.

Martin H and Moyen JF (2002) Secular changes in tonalite-trondhjemite-granodiorite composition as markers of the progressive cooling of Earth. *Geology* **30**, 319–22.

Martin H, Moyen JF, Guitreau M, Blichert-Toft J and Le Pennec JL (2014) Why Archaean TTG cannot be generated by MORB melting in subduction zones. *Lithos* **198**, 1–13.

Martin H, Moyen JF and Rapp PR (2009) The sanukitoid series: magmatism at the Archaean-Proterozoic transition. *Earth and Environmental Science Transactions of the Royal Society of Edinburgh* **100**, 15–33.

Martin H, Smithies RH, Rapp R, Moyen JF and Champion D (2005) An overview of adakite, tonalite-trondhjemite-granodiorite (TTG), and sanukitoid: relationships and some implications for crustal evolution. *Lithos* **79**, 1–24.

Moyen JF (2009) High Sr/Y and La/Yb ratios: the meaning of the "adakitic signature". *Lithos* **112**, 556–74.

Moyen JF (2011) The composite Archaean grey gneisses: petrological significance, and evidence for a non-unique tectonic setting for Archaean crustal growth. *Lithos* **123**, 21–36.

Moyen JF and Stevens G (2006) Experimental constraints on TTG petrogenesis: implications for Archean geodynamics. In *Archean Geodynamics and Environments* (eds K Benn, JC Mareschal and KC Condie), pp. 149–78. American Geophysical Union, Geophysical Monograph vol. 164. Washington, DC, USA.

Nagel TJ, Hoffmann JE and Münker C (2012) Generation of Eoarchean tonalite-trondhjemite-granodiorite series from thickened mafic arc crust. *Geology* **40**, 375–8.

Nair R and Chacko T (2008) Role of oceanic plateaus in the initiation of subduction and origin of continental crust. *Geology* **36**, 583–6.

Nutman AP, Wan YS, Du LL, Friend CRL, Dong CY, Xie HQ, Wang W, Sun H and Liu D (2011) Multistage late Neoarchaean crustal evolution of the North China Craton, eastern Hebei. *Precambrian Research* **189**, 43–65.

Nutman AP, Wan YS and Liu DY (2009) Integrated field geological and zircon morphology evidence for ca.3.8 Ga rocks at Anshan: comment on "Zircon U–Pb and Hf isotopic constraints of the early Archean crustal evolution in Anshan of the North China Craton" by Wu et al. [Precambrian Res. 167 (2008) 339–362]. *Precambrian Research* **172**, 357–60.

Peacock SM, Rushmer T and Thompson AB (1994) Partial melting of subducting oceanic crust. *Earth and Planetary Science Letters* **121**, 227–44.

Petford N and Atherton M (1996) Na-rich partial melts from newly underplated basaltic crust: the Cordillera Blanca Batholith, Peru. *Journal of Petrology* **37**, 1491–521.

Qian XL and Li JH (1999) Discovery of Neoarchean unconformity and its implication for continental cratonization of North China Craton. *Science in China* **29**, 1–8.

Rapp R, Norman M, Laporte D, Yaxley G, Martin H and Foley S (2010) Continent formation in the Archean and chemical evolution of the cratonic lithosphere: melt–rock reaction experiments at 3–4 GPa and petrogenesis of Archean Mg-diorites (sanukitoids). *Journal of Petrology* **51**, 1237–66.

Rapp RP, Shimizu N and Norman MD (2003) Growth of early continental crust by partial melting of eclogite. *Nature* **425**, 605–9.

Rapp R, Shimizu N, Norman M and Applegate G (1999) Reaction between slab-derived melts and peridotite in the mantle wedge: experimental constraints at 3.8 GPa. *Chemical Geology* **160**, 335–56.

Rapp RP and Watson EB (1995) Dehydration melting of metabasalt at 8–32 kbar: implications for continental growth and crust-mantle recycling. *Journal of Petrology* **36**, 891–931.

Rapp RP, Watson EB and Miller CF (1991) Partial melting of amphibolite/eclogite and the origin of Archean trondhjemites and tonalites. *Precambrian Research* **51**, 1–25.

Rollinson HR (1993) *Using Geochemical Data: Evaluation, Presentation, Interpretation.* Singapore: Longman Singapore Publishers (Pte) Ltd, 352 pp.

Santosh M (2010) Assembling North China Craton within the Columbia supercontinent: the role of double-sided subduction. *Precambrian Research* **178**, 149–67.

Santosh M, Liu SJ, Tsunogae T and Li JH (2012) Paleoproterozoic ultrahigh-temperature granulites in the North China Craton: implications for tectonic models on extreme crustal metamorphism. *Precambrian Research* **222**, 77–106.

Santosh M, Sajeev K and Li JH (2006) Extreme crustal metamorphism during Colombia supercontinent assembly: evidence from North China Craton. *Gondwana Research* **10**, 256–66.

Santosh M, Wan YS, Liu DY, Dong CY and Li JH (2009) Anatomy of zircons from an ultra-hot orogen: suturing the North China Craton within Columbia supercontinent. *Journal of Geology* **117**, 429–43.

Santosh M, Wilde SA and Li JH (2007) Timing of Paleoproterozoic ultrahigh-temperature metamorphism in the North China Craton: evidence from SHRIMP U–Pb zircon geochronology. *Precambrian Research* **159**, 178–96.

Santosh M, Zhao DP and Kusky TM (2010) Mantle dynamics of the Paleoproterozoic North China Craton: a perspective based on seismic tomography. *Journal of Geodynamics* **49**, 39–53.

Shan H, Zhai M and Dey S (2016) Petrogenesis of two types of Archean TTGs in the North China Craton: a case study of intercalated TTGs in Lushan and non-intercalated TTGs in Hengshan. *Acta Geologica Sinica (English Edition)* **90**, 2049–65.

Smithies R (2000) The Archaean tonalite-trondhjemite-granodiorite (TTG) series is not an analogue of Cenozoic adakite. *Earth and Planetary Science Letters* **182**, 115–25.

Söderlund U, Patchett PJ, Vervoort JD and Isachsen CE (2004) The ^{176}Lu decay constant determined by Lu–Hf and U–Pb isotope systematics of Precambrian mafic intrusions. *Earth and Planetary Science Letters* **219**, 311–24.

Song B, Nutman AP, Liu DY and Wu JS (1996) 3800 to 2500 Ma crustal evolution in Anshan area of Liaoning Province, northeastern China. *Precambrian Research* **78**, 79–94.

Springer W and Seck HA (1997) Partial fusion of basic granulites at 5 to 15 kbar: implications for the origin of TTG magmas. *Contributions to Mineralogy and Petrology* **127**, 30–45.

Trap P, Faure M, Lin W, Bruguier O and Monie P (2008) Contrasted tectonic styles for the Paleoproterozoic evolution of the North China Craton: evidence for a ~2.1 Ga thermal and tectonic event in the Fuping massif. *Journal of Structural Geology* **30**, 1109–23.

Trap P, Faure M, Lin W, Monie P, Meffre S and Melleton J (2009) The Zanhuang Massif, the second and eastern suture zone of the Paleoproterozoic Trans-North China Orogen. *Precambrian Research* **172**, 80–98.

Wan YS, Liu DY, Dong CY, Nutman A, Wilde SA, Wang W, Xie HQ, Yin XY and Zhou HY (2009a) The oldest rocks and zircons in China. *Acta Petrologica Sinica* **25**, 1793–807 (in Chinese with English abstract).

Wan YS, Liu DY, Dong CY, Xu ZY, Wang ZJ, Wilde SA, Yang YH, Liu ZH and Zhou HY (2009b) The Precambrian Khondalite Belt in the Daqingshan area, North China Craton: evidence for multiple metamorphic events in the Palaeoproterozoic era. In *Palaeoproterozoic Supercontinents and Global Evolution* (eds SM Reddy, R Mazumder, DAD Evans and AS Collins), pp. 73–97. Journal of the London Geological Society, Special Publication no. 323.

Wan YS, Song B, Liu DY, Wilde SA, Wu JS, Shi YR, Yin XY and Zhou HY (2006) SHRIMP U–Pb zircon geochronology of Paleoproterozoic metasedimentary rocks in the North China Craton: evidence for a major Late Palaeoproterozoic tectonothermal event. *Precambrian Research* **149**, 249–71.

Wang F, Li XP, Chu H and Zhao GC (2011) Petrology and metamorphism of khondalites from Jining Complex in the North China Craton. *International Geology Review* **53**, 212–29.

Wang Q, Xu JF, Jian P, Bao ZW, Zhao ZH, Li CF, Xiong XL and Ma JL (2006) Petrogenesis of adakitic porphyries in an extensional tectonic setting, Dexing, South China: implications for the genesis of porphyry copper mineralization. *Journal of Petrology* **47**, 119–44.

Whalen JB, Percival JA, McNicoll VJ and Longstaffe FJ (2002) A mainly crustal origin for tonalitic granitoid rocks, Superior Province, Canada: implications for late Archean tectonomagmatic processes. *Journal of Petrology* **43**, 1551–70.

Willbold M, Hegner E, Stracke A and Rocholl A (2009) Continental geochemical signatures in dacites from Iceland and implications for models of early Archaean crust formation. *Earth and Planetary Science Letters* **279**, 44–52.

Wu JS, Geng YS, Shen QH, Wan YS, Liu DY and Song B (1998) *Archaean Geology Characteristics and Tectonic Evolution of China-Korea Paleo-Continent.* Beijing: Geological Publishing House, 212 pp. (in Chinese)

Wu CH, Li SX and Gao JF (1986) Archean and Paleoproterozoic metamorphic regions in the North China Craton. In *Metamorphism and Crustal Evolution of China* (ed. SB Dong), pp. 53–89. Beijing: Geological Publishing House (in Chinese).

Wu FY, Zhang YB, Yang JH, Xie LW and Yang YH (2008) Zircon U–Pb and Hf isotopic constraints on the Early Archean crustal evolution in Anshan of the North China Craton. *Precambrian Research* **167**, 339–62.

Wu M, Zhao G, Sun M, Yin C, Li S and Tam PY (2012) Petrology and *P–T* path of the Yishui mafic granulites: implications for tectonothermal evolution of the western Shandong complex in the eastern block of the North China Craton. *Precambrian Research* **222–223**, 312–24.

Xia XP, Sun M, Zhao GC and Luo Y (2006a) LA-ICP-MS U–Pb geochronology of detrital zircons from the Jining complex, North China Craton and its tectonic significance. *Precambrian Research* **144**, 199–212.

Xia XP, Sun M, Zhao GC, Wu FY, Xu P, Zhang J and He YH (2008) Paleoproterozoic crustal growth in the western block of the North China Craton: evidence from detrital zircon Hf and whole rock Sr–Nd isotopic compositions of the khondalites from the Jining complex. *American Journal of Science* **308**, 304–27.

Xia XP, Sun M, Zhao GC, Wu FY, Xu P, Zhang JH and Luo Y (2006b) U–Pb and Hf isotopic study of detrital zircons from the Wulashan khondalites: constraints on the evolution of the Ordos Terrane, western block of the North China Craton. *Earth and Planetary of Science Letters* **241**, 581–93.

Xiao LL, Wu CM, Zhao GC, Guo JH and Ren LD (2010) Metamorphic *P–T* paths of the Zanhuang amphibolites and metapelites: constraints on the tectonic evolution of the Paleoproterozoic Trans-North China Orogen. *International Journal of Earth Sciences* **100**, 717–39.

Xiong XL (2006) Trace element evidence for growth of early continental crust by melting of rutile-bearing hydrous eclogite. *Geology* **34**, 945–48.

Xiong XL, Adam J and Green TH (2005) Rutile stability and rutile/melt HFSE partitioning during partial melting of hydrous basalt: implications for TTG genesis. *Chemical Geology* **218**, 339–59.

Xiong X, Adam J, Green TH, Niu H, Wu J and Cai Z (2006) Trace element characteristics of partial melts produced by melting of metabasalts at high pressures: constraints on the formation condition of adakitic melts. *Science in China Series D: Earth Sciences* **49**, 915–25.

Xiong X, Keppler H, Audetat A, Gudfinnsson G, Sun W, Song M, Xiao W and Yuan L (2009) Experimental constraints on rutile saturation during partial melting of metabasalt at the amphibolite to eclogite transition, with applications to TTG genesis. *American Mineralogist* **94**, 1175–86.

Yin CQ, Zhao GC, Guo JH, Sun M, Xia XP, Zhou XW and Liu CH (2011) U–Pb and Hf isotopic study of zircons of the Helanshan complex: constraints on the evolution of the Khondalite Belt in the western block of the North China Craton. *Lithos* **122**, 25–38.

Yin CQ, Zhao GC, Sun M, Xia XP, Wei CJ, Zhou XW and Leung WH (2009) LA-ICP-MS U–Pb zircon ages of the Qianlishan complex: constrains on the evolution of the Khondalite Belt in the western block of the North China Craton. *Precambrian Research* **174**, 78–94.

Zegers T and van Keken PE (2001) Middle Archean continent formation by crustal delamination. *Geology* **29**, 1083–6.

Zhai MG (2014) Multi-stage crustal growth and cratonization of the North China Craton. *Geoscience Frontiers* **5**, 457–69.

Zhai MG, Bian AG and Zhao TP (2000) The amalgamation of the supercontinent of North China Craton at the end of Neo-Archaean and its breakup during late Palaeoproterozoic and Mesoproterozoic. *Science China (Series D)* **43**, 219–32.

Zhai M and Santosh M (2011) The early Precambrian odyssey of the North China Craton: a synoptic overview. *Gondwana Research* **20**, 6–25.

Zhang JS, Dirks PHGM and Passchier CM (1994) Extensional collapse and uplift in a polymetamorphic granulite terrain in the Archean and Paleoproterozoic of North China. *Precambrian Research* **67**, 37–57.

Zhao GC (2009) Metamorphic evolution of major tectonic units in the basement of the North China Craton: key issues and discussion. *Acta Petrologica Sinica* **25**, 1772–92 (in Chinese with English abstract).

Zhao GC and Cawood PA (2012) Precambrian geology of China. *Precambrian Research* **222–223**, 13–54.

Zhao GC, Cawood PA, Wilde SA, Sun M and Lu L (2000) Metamorphism of basement rocks in the Central Zone of the North China Craton: implications for Paleoproterozoic tectonic evolution. *Precambrian Research* **103**, 55–88.

Zhao GC and Guo JH (2012) Precambrian geology of China: preface. *Precambrian Research* **222–223**, 1–12.

Zhao G, Li S, Sun M and Wilde SA (2011) Assembly, accretion, and break-up of the Paleo-Mesoproterozoic Columbia supercontinent: record in the North China Craton revisited. *International Geology Review* **53**, 1331–56.

Zhao GC, Sun M, Wilde SA and Li SZ (2005) Late Archean to Paleoproterozoic evolution of the North China Craton: key issues revisited. *Precambrian Research* **136**, 177–202.

Zhao GC, Wilde SA, Cawood PA and Lu LZ (1998) Thermal evolution of the Archaean basement rocks from the eastern part of the North China Craton and its bearing on tectonic setting. *International Geology Review* **40**, 706–21.

Zhao GC, Wilde SA, Cawood PA and Lu LZ (1999a) Thermal evolution of two textural types of mafic granulites in the North China Craton: evidence for both mantle plume and collisional tectonics. *Geological Magazine* **136**, 223–40.

Zhao GC, Wilde SA, Cawood PA and Lu LZ (1999b) Tectonothermal history of the basement rocks in the western zone of the North China Craton and its tectonic implications. *Tectonophysics* **310**, 37–53.

Zhao GC, Wilde SA, Cawood PA and Sun M (2001) Archean blocks and their boundaries in the North China Craton: lithological, geochemical, structural and *P–T* path constraints and tectonic evolution. *Precambrian Research* **107**, 45–73.

Zhao GC, Wilde SA, Guo JH, Cawood PA, Sun M and Li XP (2010) Single zircon grains record two continental collisional events in the North China craton. *Precambrian Research* **177**, 266–76.

Zhao G, Wilde SA, Sun M, Guo JH, Kröner A, Li SZ Li XP and Zhang J (2008) SHRIMP U–Pb zircon geochronology of the Huai'an complex: constraints on late Archean to Paleoproterozoic magmatic and metamorphic events in the Trans-North China Orogen. *American Journal of Science* **308**, 270–303.

Zheng YF, Xiao WJ and Zhao GC (2013) Introduction to tectonics of China. *Gondwana Research* **23**, 1189–206.